

Contents lists available at ScienceDirect

Transportation Research Part E

journal homepage: www.elsevier.com/locate/tre





Towards sustainable UAV operations: Balancing economic optimization with environmental and social considerations in path planning

Zhangchen Hu a,b,*, Heng Chen c, Eric Lyons d, Senay Solak b, Michael Zink d

- ^a College of Business and Economics, California State University, Fullerton, United States of America
- ^b Isenberg School of Management, University of Massachusetts Amherst, United States of America
- ^c College of Business, University of Nebraska-Lincoln, United States of America
- ^d College of Engineering, University of Massachusetts Amherst, United States of America

ARTICLE INFO

Keywords: Drone UAV path planning Weather evolution Emissions UAV noise Stochastic programming

ABSTRACT

Unmanned Aerial Vehicles (UAVs), i.e., drones, are expected to be widely used in various applications, such as parcel delivery and passenger transport, with the benefits of mitigating traffic congestion and reducing carbon emissions. In this paper, we study a UAV path planning problem under uncertain weather conditions, and design a data-driven dynamic decision support system for multiple types of UAVs. To this end, we categorize all relevant costs into three types, namely, economic, environmental, and social costs, and formulate a nonlinear two-stage stochastic programming model to establish optimal paths for UAV missions under weather uncertainty. We then discretize the nonlinear model and propose a tight linear approximation for the discretized problem to allow for a near real-time implementation. To quantify weather uncertainty, we propose a weather scenario generation algorithm to map ensemble-based weather forecast information to airspace blockage maps. With comprehensive computational studies through simulations, we show that our proposed stochastic approach can lower operating costs by an average of around 6%, where the savings increase as weather conditions become more severe and complex. We also find that, for missions operated by small UAVs, it is not sufficient to determine a path solely based on economic cost minimization, but it should rather be through total cost minimization, which involves environmental and social costs. Considering only the economic cost in the optimization may lead to much higher non-economic costs. However, for missions operated by large UAVs, it is sufficient to determine paths through economic cost optimization, as including environmental and social costs in the optimization process does not result in solutions that are much different from those obtained by considering only the economic costs. For both small and large UAVs, a path established solely through environmental or social cost minimization may not be economically sustainable, as doing so would imply very high economic costs.

^{*} Corresponding author at: College of Business and Economics, California State University, Fullerton, United States of America.

E-mail addresses: zhhu@fullerton.edu (Z. Hu), heng@unl.edu (H. Chen), elyons@engin.umass.edu (E. Lyons), solak@isenberg.umass.edu (S. Solak), zink@ecs.umass.edu (M. Zink).

1. Introduction

Unmanned Aerial Vehicles (UAVs), i.e., drones, are anticipated to be widely used in the near future as an alternative transportation mode to mitigate current congestion and pollution caused by ground transportation systems. The Federal Aviation Administration (FAA) has modified previous regulations to allow routine operations of UAVs over populated areas, and a traffic management system for UAVs is in the process of being developed (FAA, 2021). The FAA also approved a Massachusetts-based company to operate its first fully automated UAV flights without pilot observation (Pasztor and Ferek, 2021). Many leading companies, such as Amazon, Google, Uber, Wisk, and Airbus A-Cubed in the U.S., Ehang in China, and Lilium in Germany, have been investing in research on UAVs and related Urban Air Mobility (UAM) operations (Charlton, 2020). The economic impact due to commercial UAV-enabled services is projected to be \$30.9 billion by 2028 with an annual growth rate of around 50% (Yahoo Finance, 2021).

Currently, details on the specifics of UAV-based operations have not been completely specified. As the FAA continues to mature related concepts and regulations, it asks for more research and new technologies to support decisions before any large-scale deployment of UAVs (FAA, 2020). From an operational perspective, *UAV path planning*, which aims to develop safe and cost-efficient flight trajectories for UAVs, is of significant importance in responding to the above needs (Franco et al., 2018). Certain characteristics of UAVs make their operational settings distinct when compared to traditional airplanes. For example, UAV path planning is aimed at low-altitude airspace, which is constrained by complicated environmental factors, such as evolving weather conditions, terrain features, and buildings (Zhai et al., 2021). This is totally different from traditional airplanes, which mainly fly in high-altitude airspace with few obstacles. UAVs also have unique kinematic characteristics that are distinct from airplanes, e.g., a UAV can hover at the current location to wait for better weather conditions while airplanes cannot. Furthermore, most UAVs use battery-powered motors, which implies tighter constraints related to energy consumption and flight range. In contrast, traditional airplanes are fixed-wing aircraft powered by internal combustion engines, which are especially suitable for long flights (Franco et al., 2018). Given these types of distinctions, methods designed for traditional airplane path planning are not suitable for UAV path planning (Li et al., 2021), and a need exists for new approaches specifically supporting UAV flights.

Among various considerations that affect path planning, weather may have the most significant impact, as UAVs are sensitive to weather conditions (Thibbotuwawa et al., 2018). Furthermore, weather conditions evolve over time in a stochastic manner and may change dramatically in a short amount of time. Typical stochastic weather conditions impacting UAV path planning include wind, precipitation, and storms. Strong headwinds, for example, can create resistance to UAV movements, leading to increased energy consumption and flight risk (Kirschstein, 2020). Additionally, most conventional UAVs typically have a maximum wind speed resistance ranging from 10 to 14 m/s (Gao et al., 2021). Sudden gusts can destabilize a UAV, causing it to deviate from its intended path. As the most limiting weather event, precipitation can lead to moisture condensation on UAV electronics, reducing aerodynamic efficiency, causing errors, or even loss of functionality (Gao et al., 2021). We also consider other stochastic weather conditions, such as the mesoscale convective systems (MCS), small, brief, and weak storms that can result in short-duration heavy rainfall and lightning (NSSL, 2023). These storms can develop rapidly and exhibit randomness in terms of size and location (Battan, 1953; Foote and Mohr, 1979). This implies that a UAV may begin its mission under one set of weather conditions but encounter entirely different conditions during flight. Failing to account for the stochastic evolution of weather conditions could result in UAVs inadvertently entering areas with adverse weather. Thus, consideration of these weather dynamics and evolution is essential for the efficiency and safety of UAV operations. Other adverse weather conditions affecting UAV operations include dense fog, clouds, or haze, which can reduce visibility and increase the risk of UAVs colliding with obstacles like buildings, other aircraft, and power lines (Ranquist et al., 2017).

As in any penetration of technology in markets and related industries, another important consideration involves the economic, environmental, and social costs of UAV operations. Economically, companies expect a reduction in transportation costs from the use of UAVs (D'Andrea, 2014). In addition, environmental and social costs are important for all stakeholders, including the firms operating the UAVs, the policy makers, and society at large. Although we focus our efforts on electric UAVs, which are more commonly used and have little/no emission compared to ground vehicles, the energy to recharge UAVs may involve carbon emissions with costs varying regionally. In addition, the environmental benefits from electric UAVs depend on the characteristics of the type of use for the vehicle, e.g., mission type, payload, and traveling distance (Goodchild and Toy, 2018). Thus, UAV-based operations need to be carefully planned to reduce their energy usage and emissions (Stolaroff et al., 2018). From a social cost perspective, noise emissions are the most important consideration. A recent study by NASA finds that UAV sounds are more annoying than the noise from road vehicles (Christian and Cabell, 2017). Hence, due to UAVs' peculiar acoustic characteristics, noise is regarded as one of the significant barriers to public acceptance of UAV operations in urban areas (Torija et al., 2020). All these issues imply a significant need to capture the trade-offs between these different costs in UAV operations.

Our objective is to contribute to addressing this need by developing a decision support system for UAV path planning under the consideration of stochastic weather evolution. More specifically, we consider all related environmental, economic, and social costs, and try to provide answers to the following research questions: 1. Given uncertain weather conditions and all relevant costs, what would be a safe and effective initial path for a UAV mission? 2. As weather conditions evolve over time, how can the UAV path be updated accordingly? 3. How does the optimal path change for different UAV applications under varying operational settings? 4. How would optimal policies differ for different stakeholders in UAV operations? We address the above decision problems and model the relevant trade-offs among different costs through a two-stage stochastic programming framework. Our proposed model is dynamic and data-driven, which is able to deal with real weather data from radars and model the stochastic weather evolution. It allows for safe and effective path planning while also minimizing any involved costs during each mission.

The remainder of this paper is organized as follows. In Section 2, we describe the relevant literature, while also highlighting the specific contributions and practical implications of our study. In Section 3, we formally describe the problem framework we investigate and present our modeling approach. In Section 4, we present our two-stage stochastic programming formulation and provide a detailed discussion on how we incorporate weather information into our formulation. In Section 5, we extend the proposed stochastic path planning method from 2D to 3D. In Section 6, we perform detailed numerical experiments and sensitivity analyses to investigate the structural characteristics and practical implications of the proposed formulation. Finally, we summarize our findings and conclude the paper in Section 7.

2. Literature review

Our paper contributes to two streams of literature involving UAV operations. First, we describe the existing literature on UAV path planning, and how we add to this area of research. Second, we discuss relevant studies on cost calculations used in modeling UAV operations, as one of our key contributions involves the development and utilization of more comprehensive cost measures for UAV path planning.

2.1. Literature on UAV path planning

As one of the fundamental tasks for UAV operations, path planning involves the determination of a feasible, collision-free, and cost effective path from an origin to a destination (Aggarwal and Kumar, 2020). Recent surveys by Yang et al. (2014) and Aggarwal and Kumar (2020) suggest that the main approaches currently developed for path planning include heuristic methods and optimization models.

The heuristic techniques usually sample the workspace as a set of nodes, or other forms (e.g., cells) and do random searches to find an optimal path. Some examples of these approaches include Voronoi diagrams (Pehlivanoglu, 2012), the A* algorithm (Chen et al., 2018), and the visibility graph (Blasi et al., 2020). For example, He et al. (2022) develop a heuristic-based path planning method that decouples a multi-path planning problem into multiple sequential single path planning problems through prioritizing important delivery tasks. For each single path problem, they extend the A* algorithm by simultaneously considering energy consumption, risk, and airspace occupancy costs when searching potential paths. Although these heuristic methods are capable of establishing optimal or near-optimal paths in static environments, they cannot be directly applied to UAV path planning in dynamic environments, as these methods rely on characteristics of the environment and once the environment changes, the entire path has to be re-planned (Yu et al., 2018; D'Amato et al., 2019). In addition, one major shortcoming of the sampling-based heuristic techniques listed above is that it is hard to balance solution time efficiency and solution quality, especially in a complex environment with obstacles and uncertainties (Liu et al., 2022). These concerns underscore the need for a comprehensive understanding of heuristic methods and strategies to mitigate their limitations, ensuring their effective utilization in UAV path planning within dynamic operational environments. Similar to those sampling-based heuristic approaches, we use cell decomposition to divide the workspace into a grid and generate paths on the grid. However, unlike heuristic approaches that directly derive the deterministic path in a static environment, we consider a dynamic environment involving stochastic weather evolution within the workspace. More specifically, our method first generates a set of potential paths, and then identifies an optimal one with the least expected cost among the candidate paths under uncertainty.

Besides, there are a few studies concerning UAV navigations in urban settings, specifically using emerging deep reinforcement learning (DRL) methods. Tong et al. (2021) investigate UAV navigation in dynamic urban environments with rapidly moving obstacles, including birds and other UAVs. They introduce a distributed DRL framework to decompose the navigation task into two simple subtasks, enabling the handling of extensive interactive data generated by these obstacles and the discovery of a viable, shorter path through the obstructed terrain. By utilizing Long Short-Term Memory networks and a distinctive clipped DRL loss function, they can solve each subtask effectively and integrate them closely into a solution. Similarly, Yan et al. (2023) introduce the task-specific curriculum-based multiagent deep reinforcement learning (MADRL) approach, specifically designed to ensure collision-free flocking of multiple fixed-wing UAVs in obstacle-rich urban landscapes. Their approach, rooted in a curriculumbased multiagent deep reinforcement learning paradigm, systematically tackles the flocking challenge by dividing it into sequential subtasks. In response to the potential risks posed by unauthorized UAVs in urban airspace, Du et al. (2021) model a scenario where multiple cellular-connected UAVs engage in a pursuit-evasion game with an unauthorized UAV. They introduce a multiagent reinforcement learning approach that incorporates cellular-enabled parameter sharing and curriculum learning to tackle the problem, demonstrating enhanced capabilities in intercepting unauthorized UAVs. Similar to the above studies, our model can address potential threats posed by moving obstacles in urban environments through designating the corresponding airspace as blocked. However, as a major distinction, the dynamic environments we examine can incorporate randomness in the movements of weather conditions and other obstacles.

The other primary stream of research on path planning involves mathematical optimization models, which can further be categorized as deterministic and stochastic models. For deterministic formulations, linear programming is the most commonly used approach, where complex non-linear relationships in UAV path planning are converted into linear forms (Aggarwal and Kumar, 2020). For example, De Waen et al. (2017) implement mixed-integer linear programming to do path planning for UAV delivery missions in a 2D environment while minimizing traveling time. The authors also improve scalability and consistency by decomposing the problem into several smaller subproblems. Similarly, Saha et al. (2021) also use a mixed-integer linear programming model to design paths for a set of UAVs to execute surveillance missions. The two objectives of their study are to maximize the cumulative

probability of target detection while minimizing the total length of traveled paths. Similar to the papers described above, we also propose a mixed-integer programming model, but a stochastic version. In addition, while the above articles ignore the kinematics of UAVs to reduce model complexity, our model includes detailed kinematics-based calculations, such as speed dependent energy consumption, which makes our original model nonlinear. We then linearize these nonlinearities using various methods. Moreover, as deterministic models, they omit the dynamics of a changing environment, simplifying their model but limiting their applications in real environments.

There are a few papers that utilize stochastic models that capture relevant uncertainties when making UAV path planning decisions. Darbari et al. (2017) utilize Markov Decision Process (MDP) to model the control policy for a surveillance UAV and find an optimal path in the search space by considering the constraints on the UAV and the environment. Considering both known static (e.g., buildings) and uncertain dynamic moving obstacles (e.g., other aerial vehicles), their model can determine the optimal action for evading the obstacles in the vicinity with minimal deviation from the current path. Similarly, Yu et al. (2014) use an MDP model to predict the probable target motion in a surveillance mission, and plan paths for the tracking UAV to maximize the observation time of the target. Other stochastic optimization models also include multi-objective optimization models. Yin et al. (2017) propose a multi-objective path planning framework to explore a short and collision-free path for a UAV operating in a dynamic urban environment. More specifically, they use offline search methods to identify a suitable path under static obstacles and implement an online search algorithm to adjust the path to bypass dynamic obstacles. Note that mathematical optimization models are often advocated for their precision, capacity to deliver globally or locally optimal solutions, and rigorous formulation, enabling explicit constraint handling. These models can often generate optimal paths considering specific objectives and criteria, such as efficiency and security. However, disadvantages emerge regarding their computational intensity, particularly in dynamic settings, as well as the complexities of realistically modeling specific real-world aspects.

While the above papers provide insights on potential implementation methods for UAV path planning under dynamic environments, none of them consider the uncertainty of weather. The involved uncertainties in these papers mainly stem from the dynamic moving obstacles in the environment (e.g., other UAVs, birds) or the moving targets that need to be tracked rather than uncertain weather conditions. Weather uncertainty, especially adverse weather, can create a significant safety hazard and undoubtedly has a considerable impact on the UAV industry (Roseman and Argrow, 2020). However, little work has been performed to support path planning for UAVs that face weather related disruptions. A most relevant paper is by Thibbotuwawa et al. (2020), where the authors investigate UAV mission planning as a constraint satisfaction problem, which considers weather conditions (i.e., wind direction and speed), collision-avoidance, battery/energy consumption, and customer satisfaction. In their study, the authors subdivide the time horizon into several flying windows in which UAVs can be deployed and assume a deterministic weather forecast within every two consecutive flying windows. They then optimize UAV operations to achieve maximum delivery in each flying window based on the known weather forecast information. Similar to this study, we also aim at improving UAV path planning considering weather uncertainties, but we differ from the above paper in that we consider various weather conditions rather than the single input of wind. In addition, we utilize a stochastic optimization approach where the random nature of weather evolution is captured, while the model constructed by Thibbotuwawa et al. (2020) is deterministic. The primary weather conditions considered in our study are mesoscale convective systems, which are small, brief, and weak storms that can cause brief heavy rainfall and lightning (NSSL, 2023). In addition, they are highly unpredictable and can change rapidly, even over short periods (Battan, 1953; Foote and Mohr, 1979). To model such stochastic weather conditions, our model incorporates ensemble weather forecasts described in Section 4.3. These forecasts consist of a range of possible weather predictions that can capture convection dynamics, including its movement trend, growth, and dissipation. Instead of directly using the ensemble forecasts, we perform a mapping from the weather forecast information to realizations of potential weather blockage maps. Furthermore, our model takes into consideration the impact of other weather factors, such as wind speed, wind inclination, and air density, when calculating energy consumption and related costs in Sections 3.2 and 5. By accounting for these additional factors, we can provide a more comprehensive assessment of the potential impact of weather conditions on UAV path planning.

In addition to the studies mentioned above that focus on programming and simulation, both industry and academia conduct real-world tests. Related companies have conducted several successful real tests, demonstrating the potential for UAVs, especially in the parcel delivery industry. For instance, in 2016, DHL completed a successful three-month trial of its Parcelcopter, which autonomously transported packages between two locations in Germany (Industrial Distribution, 2016). More recently, Bell conducted test flights of its Autonomous Pod Transport 70 (APT 70) in Texas on December 2020, demonstrating its ability to carry a payload of up to 110 lbs over an 8-mile route. APT 70 also flew a preprogrammed four-mile route in North Texas on February 2021 (EVTOL, 2021). The safe and efficient performance of APT 70 in these tests makes it a promising candidate for parcel delivery, which we use as an example in our study. Additionally, Amazon, one of the main competitors in the industry, obtained a certificate for UAV delivery tests from the FAA in 2020 and later conducted tests in California and Texas (Mlot, 2022).

Similarly, academic research also employs real tests to validate proposed methods. For instance, Ahmed et al. (2016) propose three algorithms to establish and assign energy-efficient paths for a fleet of UAVs. The authors design an energy profiling experiment to determine the energy requirements for various types of UAV movements, followed by Matlab simulations to compare the performance of their algorithms. In another study, Rafanavicius et al. (2017) focus on solving the UAV path planning problem for power line inspections. They develop path-planning software that identifies feasible and shortest paths and test their custombuilt UAV on autopilot to find optimal parameter settings. They then conduct flight tests at approximately 230 ft height in a natural environment. The studies conducted by Luo et al. (2020), He et al. (2021), and Luna et al. (2022) share a similar research approach to the aforementioned works. Specifically, they propose methods or algorithms that address UAV path planning with specific considerations and assess their effectiveness through real-world UAV flights conducted in outdoor environments. While real

Table 1
Relative comparison of the existing research in UAV path planning (S is simulation, T is real test; 3D: 3D environment; Opti: Optimality; Stoc: Stochastic; Econ: Economic efficient; Environment efficient; Soci: Social efficient; Time: Time efficient; Energy efficient; x: considered).

Reference	S/T	3D	Opti	Stoc	Econ	Envi	Soci	Time	Ener
Yu et al. (2014)	S		x	x				x	
Ahmed et al. (2016)	S, T	x						x	
Rafanavicius et al. (2017)	S, T		x					x	
De Waen et al. (2017)	S		x					x	
Darbari et al. (2017)	S		x	x				x	
Yin et al. (2017)	S		x	x				x	
Yu et al. (2018)	S	x	x		x				
D'Amato et al. (2019)	S	x	x					X	
Thibbotuwawa et al. (2020)	S				x				x
Luo et al. (2020)	S, T	x	x	x				x	
Saha et al. (2021)	S		x	x				x	
He et al. (2021)	S, T	x	x	x				X	
Luna et al. (2022)	S, T		x		x			x	
He et al. (2022)	S		x		x				x
Liu et al. (2022)	S			X				x	
This paper	S	х	х	х	х	x	х	x	х

test flights can offer valuable insight into the practical applications of UAVs, they are often costly and limited in terms of range and operational flexibility due to regulations. For instance, existing rules require that UAVs be operated along pre-approved routes registered with the FAA, with no deviations permitted. Given these constraints, we conduct numerical analysis using computer simulations rather than physical experiments. By doing so, we can evaluate different approaches under consistent conditions, allowing for a more direct comparison of their effectiveness.

To comprehensively understand the above research, detailed analysis and comparison of these studies are explored in a tabular form as shown in Table 1. The comparison criteria include demonstration method, mission environment, optimality, stochasticity, cost efficiency (economic, environmental, social), time efficiency, and energy efficiency, as suggested by Aggarwal and Kumar (2020). Our analysis reveals that the majority of studies focus on short-range UAV path planning tasks, such as parcel deliveries and inspections. Although some studies incorporate stochastic methods to address dynamic and uncertain environments, only one study considers weather uncertainty. Furthermore, most studies prioritize time efficiency and aim to find the shortest and collision-free paths without considering the environmental and social impacts. Therefore, to accommodate various future demands in dynamic environments, our study proposes a stochastic model that considers weather uncertainty and can be applied to different types of tasks across different ranges.

2.2. Literature on cost calculations for UAV operations

UAV applications range from search and rescue missions, environmental protection, mailing, and delivery, to marine studies, space exploration, and other areas, as listed in the survey paper by Hassanalian and Abdelkefi (2017). As a result, varied objectives are considered in different applications and models. For example, some works focus on the minimization of mission completion time (Salama and Srinivas, 2022), while factors such as operational costs and environmental impacts are prioritized in other applications. Our discussion in this section focuses on research involving different cost calculations and considerations in UAV operations.

From an economic perspective, a number of papers focus on the cost-effectiveness of using UAVs as delivery methods. To examine the labor-saving technology of the UAV-based delivery systems, Welch (2015) sets forth a benefit-cost analytical framework by modeling the Prime Air system in Chattanooga, TN. When estimating the unit cost per package delivered, they consider two main costs: the capital cost to own a UAV and delivery cost to operate the UAV, which mostly corresponds to the average maintenance cost over the five-year lifespan of a UAV. McGuire et al. (2016) conduct an analysis looking at different areas of interest for a local department of transportation, such as bridge inspections and traffic data collection. The costs estimated in the report mainly include one-time equipment costs, traveling costs (e.g., fuel or electricity costs), and labor costs. They conclude that UAV applications can reduce costs while improving efficiency in most operations. As economic cost is one of the essential considerations in UAV operations, our study also considers such costs, including several expenses to operate a UAV, such as energy costs and mission cancellation costs. Unlike the above papers that mainly consider maintenance costs or utilize average flight costs to estimate UAV operating costs, we conduct detailed mission cost calculations for each performed mission. More specifically, we take into account different types of motions during a UAV mission and calculate the corresponding costs of varying flight phases.

Cost calculations also play an important role in UAV problems involving task assignment and routing. UAV task assignment problems are relevant for applications in logistics, military missions, and disaster relief operations, and consist of assigning a set of tasks (e.g., deliveries) to a fleet of UAVs based on specific environmental knowledge and task requirements (Karaman and Inalhan, 2008; Moon et al., 2013; Jiang et al., 2017; Miao et al., 2017; Chung et al., 2020). For example, Jiang et al. (2017) establish a task assignment model for multiple UAVs in a logistics application with time windows. The objective of their model is to minimize the total cost consisting of fixed costs, traveling expenses associated with UAV paths, and penalty costs when the UAV arrives later than

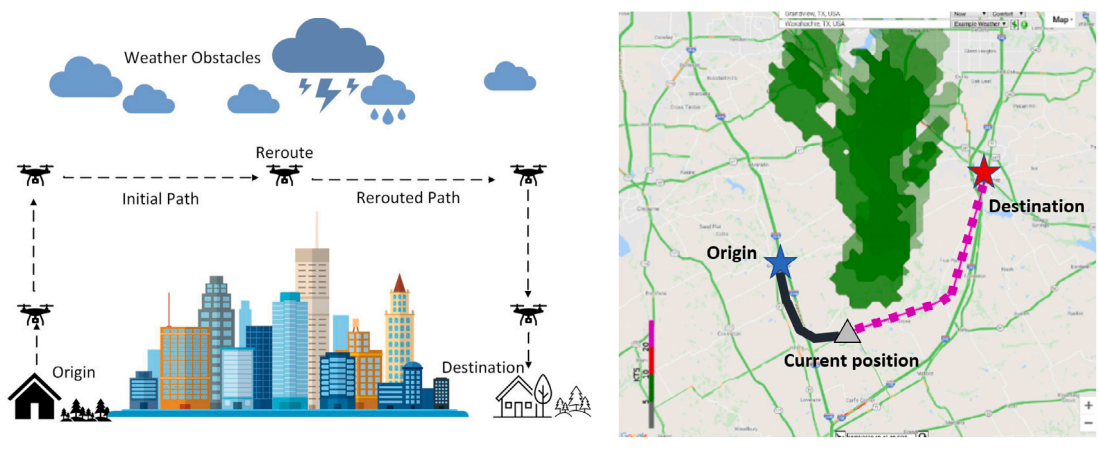
the scheduled time window. In this paper, we also take into account time windows for the missions, as a cost of mission delay is incurred if a mission arrives later than the planned completion time. Similar to the task assignment problems, the most common objectives in UAV routing problems also include minimizing operational costs and some fixed costs (e.g., the required number of UAVs) (Otto et al., 2018). Wang and Sheu (2019) propose a UAV routing problem with service hubs, where a set of trucks supply items to these hubs, and UAVs are used to deliver items to customers. The authors consider UAVs' limited flight range and capacity, and aim to minimize total logistics costs that consist of the fixed cost of employing trucks, and the transportation cost via trucks and UAVs. Unlike our paper, they assume a fixed transportation cost per unit of travel time for UAVs and trucks. As a result, the UAV transportation cost in their paper is a function of travel time, only depending on the chosen paths and the corresponding travel time along those paths. Campbell et al. (2017a) conduct a strategic analysis for the design of hybrid truck-UAV delivery systems by comparing the expected costs of hybrid truck-UAV and truck-only delivery systems. More specifically, they consider UAV operating costs and marginal UAV stop costs. For the UAV operating costs, they assume the traveling cost that a UAV incurs along a path is fixed; thus, the delivery cost is only relevant to which paths the operator chooses regardless of UAV type, weight, and speed. Shen et al. (2020) study path planning for multiple UAVs to detect ships' emissions in ports in a synergistic way. They aim to minimize the weighted sum of the total detection cost and time. For the detection cost, they mainly consider the energy cost during the flight, which is proportional to the flight distance. One major difference between the above papers and our work is that they assume fixed unit traveling costs for all UAV operations, while we consider more realistic variable mission costs. More specifically, when calculating the costs of a mission, we consider the energy costs due to different flight phases, which are complex functions of UAV speed, flight angle, payload, and wind speed. Meanwhile, we also consider the cost when a mission is cancelled either before departure or en route, which is not discussed in any of those papers.

In addition, most of these papers focus on minimizing economic costs while ignoring the impacts of UAV operations on the environment and communities. Our study extends the types of costs considered in UAV operations to include the impact on environment and communities. While there exist multiple ways to define objectives and calculate relevant costs for UAV operations, distinct from the literature, our paper takes a holistic approach to incorporate multiple types of cost structures, including fixed costs of owning a UAV, variable costs of operating a UAV considering different flight phases, delay costs of failing to meet the planned completion time, environmental costs due to carbon emissions, and social costs related to noise pollution. More specifically, the environmental costs are due to carbon emissions for providing electricity to charge UAV batteries. Thus, the environmental costs in our paper are estimated based on the total energy consumption calculated during each mission. In terms of noise costs, our calculation considers a unit noise cost per mile traveled by UAVs, which allows for adjustment via a multiplier to capture the varying noise impacts along different paths. Recognizing that these different costs represent objectives from different stakeholders, we also perform extensive numerical analyses to investigate how the changes in cost structures may affect the path planning decisions, yielding insights into how the objectives of different stakeholders may play a role in UAV path planning problems.

2.3. Contributions and major findings

To the best of our knowledge, our paper is the first study that captures the dynamic evolution of weather conditions in path planning problems for UAV missions through stochastic optimization. Although previous papers have looked at UAV path planning problems, most of them only consider static environments and economic costs. Limited research has been done to support path planning for UAVs that face probabilistically evolving weather conditions. However, the consideration of such evolving weather conditions is both necessary and practical for UAV operations, as we demonstrate the validity of weather location-dependent stochasticity from multiple dimensions in Appendix S2. Our paper contributes to this developing research area by establishing a weather scenario generation algorithm to map available ensemble-based weather forecast information to airspace blockage maps, and by proposing a two-stage stochastic programming model to identify safe and effective paths for UAV missions under weather uncertainty. In addition, the proposed stochastic programming model involves an effective and accurate approach to a nonlinear problem, which can be tightly approximated and solved through discretization and linearization procedures. Unlike other similar studies that only focus on direct operating costs, we simultaneously consider direct economic costs as well as environmental and social costs, allowing for further analysis of the balance in decisions with respect to different objectives.

From a practical perspective, the proposed method we develop throughout the paper can be easily implemented by companies involved in UAV-based operations to derive near real-time near-optimal solutions under stochastically evolving weather conditions. Throughout the paper, we obtain the following significant results and practical insights: (1) Decision makers can bear lower operational costs by implementing our proposed stochastic routing method, especially in cases where weather conditions may evolve dramatically. Based on numerical studies, our proposed stochastic framework can result in average savings of around 6% when compared with deterministic path planning models. This saving increases as weather conditions become more severe and complex, up to a level of around 12%; (2) Most of the costs when performing UAV missions are due to the economic costs, especially for missions performed by large UAVs, which usually have large payloads and fly at high speeds. Therefore, to effectively reduce economic costs, decision makers should take measures to reduce the costs associated with energy usage, mission delays, and mission cancellations. Our numerical analysis in Section 6 implies that decision makers can achieve this goal by implementing the following strategies, including: recharging batteries during periods when the electricity price is low to reduce energy-related costs; canceling UAV services in regions that will be affected by future severe weather conditions; focusing on offering delivery services within appropriate distances to avoid high mission cancellation costs; offering multiple planned completion times; and/or compensate customers for reducing mission delay costs; (3) For missions performed by small UAVs, identifying the optimal paths solely based on economic cost minimization is undesirable. Such an objective is detrimental to both economic and non-economic considerations



(a) An overview of the UAV path planning problem

(b) Example of UAV path planning

Fig. 1. UAV path planning problem.

since a tiny decrease in economic costs may result in a large increase in environmental and social costs. Thus, decisions based on total cost minimization would be a more acceptable policy with relatively low environmental and social cost levels and also a low economic cost. However, for missions performed by large UAVs, while identifying the optimal paths based on total cost minimization is still the best rule, unlike parcel delivery missions, the results of total cost minimization for passenger delivery missions are much closer to economic cost optimization. Thus, it is sufficient to determine a path through economic cost optimization. For both types of missions, it is not suggested to determine a path solely based on environmental or social cost objectives, as doing so would lead to much higher economic costs.

3. Problem description and cost functions

Consider that a UAV operator needs to plan a path for a given UAV mission, such as a parcel delivery or air taxi service in a specific region, with the objective of minimizing relevant costs while maintaining safety requirements. For simplicity, we assume without loss of generality that the UAV flies at a specific altitude h. We further divide the service region into a two-dimensional grid (X,Y) in Cartesian coordinates with I rows and J columns, where the size of each cell in the grid is determined based on weather considerations and geographical characteristics. Let $I = \{1,2,\ldots,I\}$ and $J = \{1,2,\ldots,J\}$. Each cell is referenced by the index (i,j) based on its location in the grid, where $i \in I$ and $j \in J$. Let X_i^I and X_i^U respectively denote the horizontal lower and upper bounds of cell (i,j) based on the distance of the corresponding grid lines from the vertical axis. Similarly, let Y_j^L and Y_j^U denote the vertical lower and upper bounds of cell (i,j), respectively.\(^1 In addition, the origin and the destination of a mission are respectively denoted as $o(X_o, Y_o)$ and $o(X_o, Y_o)$ and $o(X_o, Y_o)$ which are set to be located at grid points and known in advance. We note that while the above procedure is described using a two-dimensional (2D) grid structure, the approach can be extended to a three-dimensional (3D) environment if detailed 3D weather and geography information is available, as described in Section 5.

When planning paths for missions, the UAV operator needs to consider several factors. The first consideration is weather, as the flight path directly depends on weather conditions. We model the weather impacts as follows. If severe weather conditions, e.g., mesoscale convective systems, strong winds, hail, and heavy rain, exist within the airspace, the impacted cells are assumed to be blocked and unable to accommodate any flights. We also address the uncertainty and evolution of weather conditions in the considered airspace, and thus the blocked airspace and cells are random over time. The details on how we model the stochastic weather evolution are further described in Section 4.3. Note that although the blockage map structure is defined to model weather impacts, it can also be used to capture other relevant factors. For example, due to regulations, UAVs may be prohibited from flying over areas with high-density populations. In this case, these highly populated areas can be considered as additional blocked cells for path planning purposes.

The second consideration is mission-related factors such as potential delays and cancellations. To model these factors, we assume that each mission has a planned completion time Δ . If a mission takes longer than the planned completion time, it incurs a mission delay cost. In addition, if a mission is cancelled in advance or en route, and cannot arrive at its destination, a mission cancellation cost is incurred. A detailed discussion of these costs is provided in Section 3.2. Finally, the UAV operator should also ensure that the mission can be completed with the existing battery levels. This is modeled through a set of battery related constraints discussed in Section 4.

 $^{^{1}\,}$ All notation used in the paper is summarized in Appendix S1.

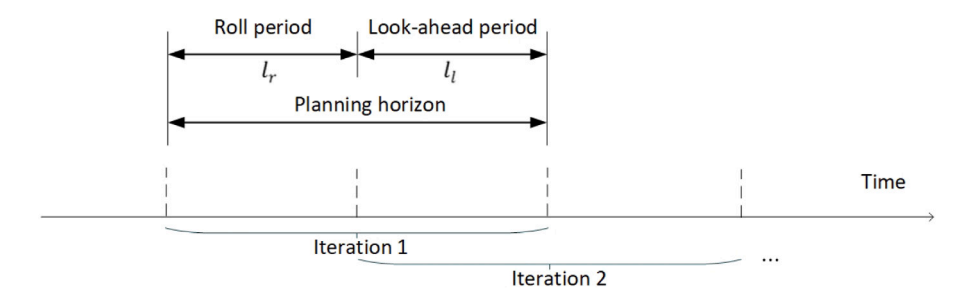


Fig. 2. Decision timeline for UAV path planning.

The UAV operator makes the routing decisions following a rolling horizon approach as shown in Fig. 2, where the decisions are based on updated weather information in an iterative manner. Such iterative routing implementations have been considered in some other studies, involving both airplane and UAV applications (Guerriero et al., 2014; Song et al., 2016; Vera et al., 2016). In these implementations, each iteration consists of two periods, also referred to as the roll and look-ahead periods in some existing literature (Samà et al., 2014; Chang et al., 2016; Yao and You, 2020; Zhan et al., 2022). Let I_r and I_l denote the duration of the two periods, respectively. It is assumed that the operator has perfect weather information for the first period (e.g., 5 min) and has an available probabilistic weather forecast for a duration after the first period (e.g., 15 min), which we refer to as the look-ahead period. The goal of each iteration is to identify the optimal initial path that the UAV can fly along during the first period based on the current observed weather and available weather forecasts. To indicate the availability status of airspace due to weather conditions, we introduce a binary parameter $b_{i,j,l}$ for each cell (i,j) during each period $t \in \{r,l\}$, where $b_{i,j,l} = 1$ if the cell is blocked during period t, and $b_{i,j,l} = 0$ otherwise.

The problem of identification of this optimal initial path during each iteration can be solved by a two-stage stochastic programming model, where the first stage decisions correspond to the selection of this path. The second stage decisions are the recourse actions to take during the second period based on realized weather information in that period. These actions, which would vary for each possible weather scenario, involve routing the UAV around realized weather or mission cancellation decisions. The optimal initial path is the option that would minimize the expected costs of operating the flight during the two periods, where the expectation is defined by the probabilities of weather scenarios.

The next iteration is implemented after performing the optimal decisions of the first period. The UAV operator again observes the current weather conditions, as well as the weather forecast for the new look-ahead period, and decides on the next optimal leg for the mission via the two-stage stochastic programming model. An example of the UAV path planning problem is shown in Fig. 1(b). The solid line represents the path established in previous iterations that the UAV has already flown from the origin to its current position, while the dashed line indicates a potential path established based on the current iteration, representing one of the various paths the UAV could take to reach its destination from its current position.

3.1. Model setup

As noted above, the decision problem in each iteration of the rolling horizon implementation can be represented by a twostage stochastic programming model. To this end, we model the weather uncertainty during the second period of each iteration by considering a scenario set Ω with a probability p_{ω} associated with each scenario $\omega \in \Omega$. Each scenario characterizes the predicted weather conditions of the service region during that period. The details on how we implement weather forecasts to generate such a scenario set are discussed in Section 4.3.

Using current and predicted weather information, the following set of decisions will be made during the first period of each iteration, where the UAV operator decides whether or not to operate the current mission at the beginning of the period. If the mission continues, the UAV operator establishes an initial path to move forward from the current position $\mathbf{p}_1=(X_1,Y_1)$ and sets a flight speed for the UAV to fly along that path. To do so, the UAV operator picks a waypoint where the UAV is to arrive at the end of that period, denoted as $\mathbf{p}_2=(X_2,Y_2)$, and generates a corresponding initial path, represented as $\vec{D}_{1,2}$. Note that multiple potential waypoints within the range of UAV flight are considered and searched when identifying the optimal waypoint. We let $N_{i,j}$ denote the length of path $\vec{D}_{i,j}$, which is the Euclidean distance between point \mathbf{p}_i and point \mathbf{p}_j , and let $V_{i,j}$ denote the set flight speed along path $\vec{D}_{i,j}$. The UAV operator can also decide for the UAV to hover at its current position during the first period to wait for better weather conditions to continue the flight. In that case, the UAV will stay at the current position until the end of the first period, i.e., $\mathbf{p}_2=\mathbf{p}_1$ and $N_{1,2}=0$. Second, if an en route mission is cancelled, the operator establishes a path $\vec{D}_{1,o}$ between its current position \mathbf{p}_1 and its origin o, then directs the UAV back to the origin at a fixed average flight speed \bar{v} . We use a binary variable Y_1 to denote the decision as to whether or not to operate the current mission. If the mission is to be cancelled, then $Y_1=1$; otherwise, $Y_1=0$.

Similarly, a set of second-stage recourse decisions are assumed to be made for the second period after the realization of weather uncertainty, which also includes mission cancellation, path generation, and speed decisions. Let Y_2^ω denote whether or not to cancel the mission during the second period under scenario $\omega \in \Omega$, where $Y_2^\omega = 1$ if the current mission is cancelled, and $Y_2^\omega = 0$ otherwise.

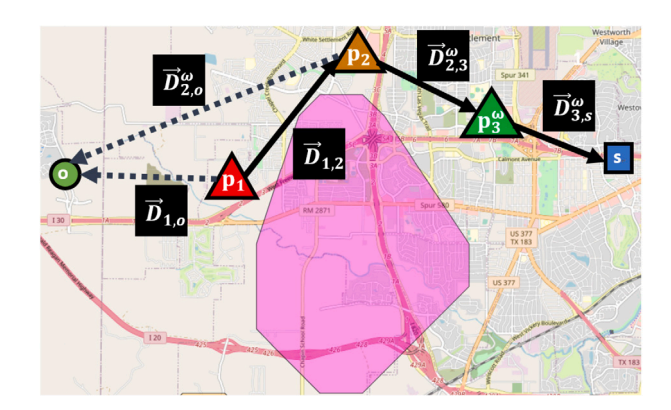


Fig. 3. Example of path generation overview (o: origin, s: destination; \mathbf{p}_1 : current position of UAV; $\mathbf{p}_2, \mathbf{p}_3$: final chosen waypoints during the first and second periods, respectively; $\vec{D}_{1,o}$: return path between \mathbf{p}_1 and origin o in the event of cancellation; $\vec{D}_{2,o}^{w}$: return path between \mathbf{p}_2 and origin o in the event of cancellation under scenario o; $\vec{D}_{1,2}$: established initial path between \mathbf{p}_1 and \mathbf{p}_2 during the first period; $\vec{D}_{2,3}^{w}$: established path between \mathbf{p}_2 and \mathbf{p}_3^{w} under scenario o during the second period; $\vec{D}_{3,s}^{w}$: path that the UAV would follow after the second period until destination s).

If the mission is not to be cancelled, a waypoint $\mathbf{p}_3^\omega = (X_3^\omega, Y_3^\omega)$ is selected for the UAV to arrive at the end of the second period. This waypoint \mathbf{p}_3^ω is selected from a set of potential options located around waypoint \mathbf{p}_2 within the range of UAV flight after conducting a thorough search. The established path between \mathbf{p}_2 and \mathbf{p}_3^ω under scenario ω can be expressed as $\vec{D}_{2,3}^\omega$. Note that as previously mentioned, the recourse actions for the second stage, such as selecting waypoint \mathbf{p}_3^ω , will not be implemented during the current iteration. Instead, the operator utilizes these actions to estimate the costs associated with selecting waypoint \mathbf{p}_2 more accurately during the first period. It is important to note that a new iteration begins once the UAV reaches \mathbf{p}_2 , and the operator can decide whether to cancel the mission based on updated weather information. Therefore, we do not consider mission cancellation at waypoint \mathbf{p}_2^ω during the current iteration.

In addition, the operator also needs to identify the path that the UAV would follow after the second period until the destination s, denoted as $\vec{D}_{3,s}^{\omega}$, which is established based on the waypoint \mathbf{p}_3^{ω} and the weather conditions under scenario ω . Let $N_{2,s}^{\omega}$ denote the traveling distance that the UAV flies along the paths $\vec{D}_{2,3}^{\omega}$ and $\vec{D}_{3,s}^{\omega}$, where $N_{2,s}^{\omega} = N_{3,s}^{\omega}$. Finally, the operator sets a new flight speed for the UAV to fly along the path during the second period, denoted as $V_{2,3}^{\omega}$, while the flight speed after the current period is approximated by the average speed \bar{v} . If the mission is to be cancelled, we let $\vec{D}_{2,o}^{\omega}$ represent the established return path between the current position \mathbf{p}_2 and its origin o under scenario ω . In order to consider potential changes in weather conditions, the return path $\vec{D}_{2,o}^{\omega}$ is established by using the blockage map that corresponds to the weather forecast under scenario ω . Similar to the first stage, the UAV is to fly at the fixed average speed \bar{v} along the return path. An example of how the operator establishes and updates paths is shown in Fig. 3, where the shaded polygon denotes the blocked airspace due to severe weather conditions in one scenario. Note that Fig. 3 depicts one of these recourse actions based on one of the possible weather scenarios. For demonstration purposes, Fig. 3 only shows the finally chosen waypoint (e.g., \mathbf{p}_2 , \mathbf{p}_3^{ω}) for each period. However, a set of potential waypoints are considered and actually searched when identifying the optimal waypoint of each period. This process is not shown in Fig. 3, but it is explained in detail in Section 4.1.

3.2. Cost functions

As part of our modeling framework, we categorize all relevant costs incurred by a mission into three different types of costs: economic, environmental, and social costs. We describe each of these in the following sections.

3.2.1. Economic costs

For economic costs (cost eco.), we include energy usage costs, as well as mission delay and cancellation costs.

Energy usage costs: Energy usage costs for a UAV mission depend on the type of movement for the UAV, as hovering and horizontal movements incur different costs. To this end, we calculate the energy consumption and the resulting costs for each movement type separately.

The energy usage cost $C_{energy}(N_{i,j})$ when a UAV flies horizontally along a path $\vec{D}_{i,j}$ with length $N_{i,j}$ at flight speed $V_{i,j}$ is calculated based on the total energy consumption and the unit electricity price c_{EN} . According to Aiello et al. (2021), we have:

$$C_{energy}(N_{i,j}) = c_{EN} \frac{E_{i,j}}{n},\tag{1}$$

where η is a given overall efficiency factor that measures the combined efficiency of battery charging and discharging. On the other hand, E_{ij} denotes the theoretical energy consumption when the UAV flies along the selected path, defined as:

$$E_{i,j} = \begin{cases} P_{hor}(V_{i,j}) \cdot l_r, & i = 1, j = 2, V_{i,j} = \frac{N_{i,j}}{l_r} \\ P_{hor}(V_{i,j}) \cdot l_l, & i = 2, j = 3, V_{i,j} = \frac{N_{i,j}}{l_l} \\ P_{hor}(\bar{v}) \cdot \frac{N_{i,j}}{\bar{v}}, & i \in \{1,2\}, j = o \text{ or } i = 3, j = s, \end{cases}$$

$$(2)$$

where $P_{hor}(\cdot)$ denotes the unit amount of energy consumed for horizontal motion, which we define in more detail below. In Eq. (2), $P_{hor}(V_{1,2}) \cdot I_r$ and $P_{hor}(V_{2,3}) \cdot I_l$ denote the energy consumption when the UAV continues the mission and flies along selected paths $\vec{D}_{1,2}$ and $\vec{D}_{2,3}$, respectively. Note that $N_{i,j}$ and $V_{i,j}$ are related variables in the above two cases: as the durations of the two periods are fixed, whenever the operator decides to continue the mission and selects a path for a period, the corresponding flight speed of that period is also known, i.e., $V_{1,2} = \frac{N_{1,2}}{l_r}$ and $V_{2,3} = \frac{N_{2,3}}{l_l}$. In addition, $P_{hor}(\bar{v}) \cdot \frac{N_{i,j}}{\bar{v}}$ defines the energy consumption when the UAV flies along the return path, i.e $\vec{D}_{i,o}$, or the path that the UAV would follow after the second period until the destination, i.e $\vec{D}_{3.s}$. As the UAV is to fly at the fixed average speed along these paths, $\frac{N_{i,j}}{\bar{b}}$ defines the horizontal flight time. As noted above, $P_{hor}(V_{i,j})$ denotes the unit amount of energy consumed for horizontal motion when the UAV flies at flight speed

 $V_{i,i}$, and is calculated by the following formula (Aiello et al., 2021):

$$P_{hor}(V_{i,j}) = \frac{1}{2}c_D s_f \rho (\sqrt{(V_{i,j} \cdot \cos\beta_{i,j} + v_{i,j}^{wd} \cdot \cos\beta_{i,j}^{wd})^2 + (V_{i,j} \cdot \sin\beta_{i,j} + v_{i,j}^{wd} \cdot \sin\beta_{i,j}^{wd})^2})^3 + \sqrt{\frac{(m_0 + m_p)^3 g^3}{2\rho s_f}}$$
 (3)

where c_D is the aerodynamic drag coefficient, s_f is the UAV front surface area, m_0 is the UAV mass, m_p is the payload mass, ρ is air density, g is gravitational acceleration, and $\sqrt{(V_{i,j}\cdot\cos\beta_{i,j}+v_{i,j}^{wd}\cdot\cos\beta_{i,j}^{wd})^2+(V_{i,j}\cdot\sin\beta_{i,j}+v_{i,j}^{vd}\cdot\sin\beta_{i,j}^{wd})^2}$ is the relative speed of the UAV, considering flight speed $V_{i,j}$ and inclination angle of flight $\beta_{i,j}$, wind speed $v_{i,j}^{wd}$ and inclination angle $\beta_{i,j}^{wd}$ of wind during the flight along path $\vec{p}_{i,j}$. We note that $P_{hor}(V_{i,j})$ is a convex function with respect to $V_{i,j}$, since $P''_{hor}(V_{i,j}) = \frac{3}{2}c_D s_f \rho(\frac{(1+(\sin\beta_{i,j}\sin\beta_{i,j}^{wd}+\cos\beta_{i,j}\cos\beta_{i,j}^{wd})\cdot v_{i,j}^{wd})^2}{\sqrt{(V_{i,j}\cos\beta_{i,j}+v_{i,j}^{wd}\cos\beta_{i$

 $c_{EN} \frac{P_{hor}(0) \cdot l_r}{r}$, which is a special case of the energy usage cost of horizontal movement when the UAV flight speed is set to 0 during the same period, i.e., $V_{i,j} = 0$ and $N_{i,j} = 0$.

Mission delay costs: We assume that, if a mission takes longer than a planned completion time Δ_e from the current position to complete during iteration e, then the service provider will incur a cost of c_W per unit of time that the mission delivery is delayed beyond Δ_e . Without loss of generality, we assume the planned completion time of a mission during iteration e is a function of the distance between the current position \mathbf{p}_1 and destination s, calculated as $\Delta_e = \frac{N_{1,s}}{\bar{v}}$, where \bar{v} is the average flight speed. Given this, the cost of mission delay can be expressed as:

$$C_{delay}(N_{2,s}) = c_W \max(l_r + \frac{\sum_{\omega \in \Omega} p_\omega \cdot N_{2,s}^\omega}{\bar{p}} - \Delta_e, 0)$$

$$\tag{4}$$

where $l_r + \frac{\sum_{\omega \in \Omega} p_\omega \cdot N_{2,s}^\omega}{n}$ denotes the expected arrival time to complete the current mission. More specifically, l_r is the duration of the first period, $\sum_{\omega \in \Omega} p_{\omega} \cdot N_{2s}^{\omega}$ is the expected total flight distance that the UAV flies from the waypoint \mathbf{p}_2 to destination s.

Mission cancellation costs: If a mission is cancelled before departure, it incurs a fixed cancellation cost for each advancecancelled mission, defined as c_{MC} . The value of c_{MC} varies based on the mission type. For example, a higher cancellation cost can be assigned to urgent medical missions, compared to regular retail deliveries. Similarly, an en-route mission may be cancelled at the beginning of a period, and the UAV would be required to fly back to its origin. The corresponding en route mission cancellation cost $C_{cancel}(N_{i,o})$ is determined as:

$$C_{cancel}(N_{i,o}) = c_{MC} + C_{energy}(N_{i,o}), \tag{5}$$

where $N_{i,o}$ represents the traveling distance for returning/diverting from current position \mathbf{p}_i to its origin o, $C_{energy}(N_{i,o})$ is the energy usage cost due to cancellation and returning as defined in Eq. (1). Based on the above cost structures, we can express the total economic cost incurred by the path established during each period as:

$$cost_{eco}(N_{i,j}) = \begin{cases} C_{cancel}(N_{i,o}), & i \in \{1,2\} \\ C_{energy}(N_{i,j}), & i = 1, j = 2 \\ \sum_{(i',j') \in \{(2,3),(3,s)\}} \{C_{energy}(N_{i',j'})\} + C_{delay}(N_{i,j}), & i = 2, j = s. \end{cases}$$

$$(6)$$

In this representation, if the mission is to be cancelled at the beginning of either period and the UAV flies along the return path $\bar{D}_{i,o}$. the incurred economic cost is the mission cancellation cost $C_{cancel}(N_{i,o})$. When the mission continues during the first period and the UAV flies along the selected path $\vec{D}_{1,2}$, the incurred economic cost only includes the energy usage cost $C_{energy}(N_{1,2})$. Finally, when the mission continues during the second period and the UAV flies along the selected path $\vec{D}_{2,3}$ and $\vec{D}_{3,5}$, the incurred economic cost consists of energy usage cost $\sum_{(i,i)\in\{(2,3),(3,s)\}}\{C_{energy}(N_{i,j})\}$ and mission delay cost $C_{delay}(N_{2,s})$.

3.2.2. Environmental costs

While electric UAVs do not generate carbon emissions directly, the source to charge/recharge them, for example, fossil power facilities, can cause emissions and introduce indirect environmental costs of operating UAVs, which we aim to quantify in this section. Similar to the calculation of energy consumption, we calculate the CO₂ emissions for each motion type separately.

The emission-related cost due to horizontal movement along path $\vec{D}_{i,j}$, denoted as $cost_{env}(N_{i,j})$, is calculated according to the unit cost of CO_2 emissions c_{EM} and the amount of CO_2 emitted for power generation, such that:

$$cost_{env}(N_{i,j}) = c_{EM} \xi_{grid} \frac{E_{i,j}}{\eta \cdot \eta_g}, \tag{7}$$

where ξ_{grid} is the CO₂ marginal emission rate which measures the CO₂ emitted at power generation facilities per kWh consumed by a UAV (Goodchild and Toy, 2018). On the other hand, $\frac{E_{i,j}}{\eta \cdot \eta_g}$ calculates the amount of electricity that needs to be generated at the power facilities for a UAV to receive usable electricity from the UAV battery, where η is the combined efficiency of battery charging and discharging, and η_g is the efficiency of transmission and distribution on the grid (Stolaroff et al., 2018).

Similarly, the total emission-related cost for hovering during the first period is a special case of the total emission-related cost for horizontal movement when the UAV flight speed is set to 0 during the same period, calculated as $cost_{env}(0) = c_{EM} \xi_{grid} \frac{P_{hor}(0) \cdot l_r}{\eta \cdot \eta_\sigma}$.

3.2.3. Social costs

Transportation, including road, rail, and air, can generate noise pollution and cause significant negative social implications from two distinct aspects (Maibach et al., 2008). The first is a cost of annoyance, since transportation noise imposes undesired social disturbances resulting in social and economic costs. The second is the health costs, as transportation noise can cause physical health damage. For example, noise levels above 85 dBA cause hearing damage, while noise levels between 60 dBA and 84 dBA may lead to nervous stress reactions. Several studies in the literature have already estimated the marginal noise cost of different transportation types considering both implications (Levinson et al., 1999; Maibach et al., 2008; Eurocontrol, 2020). However, an estimate of UAVs' noise costs has not been well-established, and a similar analysis is required to estimate UAVs' environmental and social impacts compared to conventional transportation modes (EASA, 2019). As an approximation, we use the marginal noise costs defined for traditional aircraft from the above literature, and estimate the total noise-related costs along any path $\vec{D}_{i,i}$ by:

$$cost_{NOC}(N_{i,i}) = c_{NO}\zeta_{NO}N_{i,i}, \tag{8}$$

where c_{NO} is the unit noise cost per mile traveled. Since different paths may lead flights over various areas (e.g., urban areas vs. suburban areas), the noise impact when a UAV flies along those paths also varies. Therefore, we approximate the difference in noise impacts among those paths by assigning different noise coefficients, denoted as ζ_{NO} . This approximation offers an opportunity to estimate the social impact of UAVs due to noise pollution. In addition, based on a recent report from Rizzi et al. (2020), a challenge unique to UAV noise is that different UAVs may have entirely different acoustic signatures due to design characteristics. Thus we consider various noise cost parameters and perform sensitivity analysis in Section 6 to account for any inaccuracy in the approximations.

4. Model formulation and scenario generation

In this section, we first express the total cost incurred by the path established for each period based on the above cost structures, then formulate the two-stage stochastic programming model to be solved during each iteration with the objective of minimizing expected costs. The total cost $cost_{tot}(N_{i,j})$ incurred by the selected path $\vec{D}_{i,j}$ can be denoted as $cost_{tot}(N_{i,j}) = cost_{eco}(N_{i,j}) + cost_{env}(N_{i,j}) + cost_{soc}(N_{i,j}), \forall (i,j) \in \{(1,2),(1,o),(2,3),(2,o),(3,s)\}$. Given the above definitions, the stochastic programming model to identify an initial path that minimizes the total expected cost of the flight over the first period of each iteration can be expressed as follows:

$$\min \quad Y_{1} \cdot cost_{tot}(N_{1,o}) + (1 - Y_{1}) \cdot cost_{tot}(N_{1,2}) + \sum_{\omega \in \Omega} p_{\omega} \{ Y_{2}^{\omega} \cdot cost_{tot}(N_{2,o}^{\omega}) + (1 - Y_{1} - Y_{2}^{\omega}) \cdot cost_{tot}(N_{2,s}^{\omega}) \}$$

$$(9)$$

s.t.
$$N_{1,2} \ge \sqrt{(X_2 - X_1)^2 + (Y_2 - Y_1)^2}$$
 (10)

$$N_{2,3}^{\omega} \ge \sqrt{(X_3^{\omega} - X_2)^2 + (Y_3^{\omega} - Y_2)^2}, \quad \forall \omega \in \Omega$$
 (11)

$$N_{3,c}^{\omega} \ge \sqrt{(X_2^{\omega} - X_s)^2 + (Y_2^{\omega} - Y_s)^2}, \quad \forall \omega \in \Omega$$
 (12)

$$N_{2,s}^{\omega} = N_{2,s}^{\omega} + N_{3,s}^{\omega}, \quad \forall \omega \in \Omega$$

$$(13)$$

$$V_{1,2} = \frac{N_{1,2}}{I_r} \tag{14}$$

$$V_{2,3}^{\omega} = \frac{N_{2,3}^{\omega}}{l_l}, \quad \forall \omega \in \Omega$$
 (15)

$$V_{1,2} \leq v_{max}$$
 (16)

$$V_{2,2}^{\omega} \le v_{max}, \quad \forall \omega \in \Omega$$
 (17)

$$E_{1,2} = P_{hor}(V_{1,2}) \cdot l_r \tag{18}$$

$$E_{2,o}^{\omega} = P_{hor}(\bar{v}) \cdot \frac{N_{2,o}^{\omega}}{\bar{v}}, \quad \forall \omega \in \Omega$$
 (19)

$$E_{2,s}^{\omega} = P_{hor}(V_{2,3}^{\omega}) \cdot l_l + P_{hor}(\bar{v}) \cdot \frac{N_{3,s}^{\omega}}{\bar{v}}, \quad \forall \omega \in \Omega$$
 (20)

$$\max(P_{hor}(\bar{v}) \cdot \frac{N_{1,o}}{\bar{v}}, E_{1,2}) + \max(E_{2,o}^{\omega}, E_{2,s}^{\omega}) \le \eta \cdot Cap_e^B, \quad \forall \omega \in \Omega$$

$$Y_{\alpha}^{o} \le 1 - Y_{1}, \quad \forall \omega \in \Omega$$
 (22)

$$(X_2, Y_2) \in \{(X_2, Y_2) | X_i^L \le X_2 < X_i^U \text{ and } Y_i^L \le Y_2 < Y_i^U \}, \quad \forall (i, j) | b_{i,j,r} = 0, i \in \mathcal{I}, j \in \mathcal{J}$$
 (23)

$$(X_3^{\omega}, Y_3^{\omega}) \in \{(X_3^{\omega}, Y_3^{\omega}) | X_i^L \le X_3^{\omega} < X_i^U \text{ and } Y_i^L \le Y_3^{\omega} < Y_i^U \}, \quad \forall (i, j) | b_{i, i, l}^{\omega} = 0, i \in \mathcal{I}, j \in \mathcal{J}, \omega \in \Omega$$
 (24)

$$Y_1, Y_2^{\omega} \in \{0, 1\}, \quad \forall \omega \in \Omega$$
 (25)

$$X_{2},Y_{2},X_{3}^{\omega},Y_{3}^{\omega},N_{1,2},N_{2,3}^{\omega},N_{3,s}^{\omega},N_{2,s}^{\omega},V_{1,2},V_{2,3}^{\omega},E_{1,2},E_{2,o}^{\omega},E_{2,s}^{\omega}\in\mathcal{R}^{+},\quad\forall\omega\in\Omega. \tag{26}$$

The objective function of the optimization model includes two parts. The first part corresponds to the costs associated with the initial path selection, while the second part involves the recourse costs after the realization of weather uncertainty. Specifically, $cost_{tot}(N_{1,o})$ and $cost_{tot}(N_{2,o}^{\omega})$ denote the cancellation cost when the mission is cancelled at the beginning of the first and second periods, respectively. On the other hand, $cost_{tot}(N_{1,2})$ and $cost_{tot}(N_{2,s}^{\omega})$ represent the total cost if the mission is continued along the chosen path during the first and second periods, respectively. Constraints (10)–(12) define the traveling distances on paths $\vec{D}_{1,2}$, $\vec{D}_{2,0}^{\omega}$, $\vec{D}_{2,3}^{\omega}$ and $\vec{D}_{3,s}^{\omega}$, respectively; while constraint (13) denotes the total traveling distance in the second period over paths $\vec{D}_{2,3}^{\omega}$ and $\vec{D}_{3,s}^{\omega}$. Constraints (14) and (15) define the flight speed of the UAV during the first and second periods, respectively. Constraints (16) and (17) indicate that the flight speed of a UAV is bounded by the maximum speed v_{max} . Constraint (18) is the energy consumption equation for the first period, while (19) and (20) are the corresponding equations for the second period, where the former applies in case of a cancellation decision. Note, we define $P_{hor}(\cdot)$ in (3). Constraint (21) ensures that the total energy consumption during the mission will not exceed the available battery level $\eta \cdot Cap_{e}^{B}$. Constraint (22) ensures that a mission can be continued during the second period only if it is not cancelled at the beginning of the first period. Constraints (23) and (24) define the coordinates of potential waypoints during each period. More specifically, these constraints indicate that only points (X,Y) that are not in a blocked cell will be considered as potential waypoints, such that $X_1^L \leq X < X_1^U$ and $Y_2^L \leq Y < Y_2^U$ if $b_{i,j,l} = 0$ in the corresponding weather observation or scenario. Finally, constr

A major challenge with the above model is the expression of the constraints (23) and (24). These constraints would require the introduction of a large number of additional binary variables and constraints to represent the if-then type relations implied by the corresponding cell blockage conditions. This would prevent the near real-time solution of the resulting large scale integer problem, especially considering that the model can potentially involve a large number of scenarios. Hence, in the following subsection, we develop a discretization and linearization based approach, which allows for an efficient solution that can be calculated and implemented in real-time.

4.1. Model discretization through path selection

For our discretization based model, we assume a finite set $\mathcal K$ of potential waypoints for the UAV to fly to within the current period from its current position, which is calculated a priori and is defined by speed limitations and the discretization factor used. To this end, we let $k \in \mathcal K$ indicate such a feasible waypoint. Note that the current position is also included in the set of feasible waypoints to represent a hovering decision. Similarly, for the second period, we let $r_k^\omega \in \mathcal R_k^\omega$ indicate a feasible waypoint reachable from point k under scenario ω during the second period, with $\mathcal R_k^\omega$ denoting the set of all these potential points. Points within blocked cells are not considered, as no safe paths can be generated through these points. Hence, the decision space of waypoints during each period is discretized and represented as finite sets of points to consider for optimization purposes. The distances corresponding to the paths to be generated through the potential points are also known and calculated a priori.

Given this representation, we formulate the discretized version of our optimization model as follows. Let binary variable Ψ_k indicate whether or not point k is selected as an optimal waypoint during the first period. If point k is selected, $\Psi_k=1$, otherwise, $\Psi_k=0$. Hence, the length of the initial path $\vec{D}_{1,2}$ can be expressed as $N_{1,2}=\sum_{k\in\mathcal{K}}\Psi_k\cdot n_{1,k}$, where $n_{1,k}$ denotes the Euclidean distance between the current position and potential point k. In addition, the UAV is to fly along the corresponding path during the first period with a constant speed $V_{1,2}=\frac{N_{1,2}}{l_r}$. Similarly, for the second period, we let binary variable $\Psi_{r_k^{\omega}}$ indicate whether or not point $r_k^{\omega}\in\mathcal{R}_k^{\omega}$ is selected as an optimal

Similarly, for the second period, we let binary variable $\Psi_{r_k^\omega}$ indicate whether or not point $r_k^\omega \in \mathcal{R}_k^\omega$ is selected as an optimal waypoint under scenario ω . If point r_k^ω is selected, $\Psi_{r_k^\omega} = 1$, otherwise, $\Psi_{r_k^\omega} = 0$. Moreover, the length of the path $\vec{D}_{2,3}^\omega$ can be expressed as $N_{2,3}^\omega = \sum_{k \in \mathcal{K}} \sum_{r_k^\omega \in \mathcal{R}_k^\omega} \Psi_{r_k^\omega} \cdot n_{k,r_k^\omega}$, where n_{k,r_k^ω} denotes the Euclidean distance between waypoint k and waypoint r_k^ω under scenario ω . The UAV is set to fly along these paths with a constant speed $V_{2,3}^\omega = \frac{N_{k,3}^\omega}{l_l}$. Note that once the waypoint is determined for

the second period, the corresponding path $\vec{D}^{\omega}_{3,s}$ that the UAV travels along after the second period under each scenario is also known. The traveling distance of that path can be denoted as $N^{\omega}_{3,s} = \sum_{k \in \mathcal{K}} \sum_{r_k^{\omega} \in \mathcal{R}_k^{\omega}} \Psi_{r_k^{\omega}} \cdot n_{r_k^{\omega},s}$, where $n_{r_k^{\omega},s}$ is the Euclidean distance between waypoint r_k^{ω} and destination s under scenario ω . Finally, if the operator decides to cancel the en-route mission in the second period, the algorithm establishes a path $\vec{D}^{\omega}_{2,o}$ for the UAV to fly from waypoint k to the origin o. To that end, we let $N^{\omega}_{2,o} = \sum_{k \in \mathcal{K}} \Psi_k \cdot n^{\omega}_{k,o}$ denote the traveling distance of the picked path $\vec{D}^{\omega}_{2,o}$.

Based on the above description, the discretization based stochastic programming model can be expressed as follows:

$$\min \quad Y_{1} \cdot cost_{tot}(N_{1,o}) + (1 - Y_{1}) \cdot cost_{tot}(N_{1,2}) + \sum_{\omega \in \Omega} p_{\omega} \{ Y_{2}^{\omega} \cdot cost_{tot}(N_{2,o}^{\omega}) + (1 - Y_{1} - Y_{2}^{\omega}) \cdot cost_{tot}(N_{2,s}^{\omega}) \}$$

$$(27)$$

s.t. Constraints (13)-(22), (25)

$$Y_1 + \sum_{k \in \mathcal{K}} \Psi_k = 1 \tag{28}$$

$$Y_2^{\omega} + \sum_{k \in \mathcal{K}} \sum_{r_{\nu}^{\omega} \in \mathcal{R}_{\nu}^{\omega}} \Psi_{r_{k}^{\omega}} = 1, \quad \forall \omega \in \Omega$$
 (29)

$$N_{1,2} = \sum_{k \in \mathcal{K}} \Psi_k \cdot n_{1,k} \tag{30}$$

$$N_{2,3}^{\omega} = \sum_{k \in \mathcal{K}} \sum_{r^{\omega} \in \mathcal{R}^{\omega}} \Psi_{r_{k}^{\omega}} \cdot n_{k,r_{k}^{\omega}}, \quad \forall \omega \in \Omega$$

$$(31)$$

$$N_{3,s}^{\omega} = \sum_{k \in \mathcal{K}} \sum_{r_k^{\omega} \in \mathcal{R}_k^{\omega}} \Psi_{r_k^{\omega}} \cdot n_{r_k^{\omega},s}, \quad \forall \omega \in \Omega$$
 (32)

$$N_{2,o}^{\omega} = \sum_{k \in \mathcal{K}} \Psi_k \cdot n_{k,o}^{\omega}, \quad \forall \omega \in \Omega$$
 (33)

$$\sum_{r_k^{\omega} \in \mathcal{R}_k^{\omega}} \Psi_{r_k^{\omega}} = \Psi_k, \quad \forall k \in \mathcal{K}, \omega \in \Omega$$
(34)

$$\Psi_k, \Psi_{r_k^{\omega}} \in \{0, 1\}, \quad \forall \omega \in \Omega$$
 (35)

$$N_{1,2}, N_{2,s}^{\omega}, N_{3,s}^{\omega}, N_{3,s}^{\omega}, N_{2,s}^{\omega}, V_{1,2}, V_{2,s}^{\omega}, E_{1,2}, E_{2,s}^{\omega}, E_{2,s}^{\omega} \in \mathcal{R}^{+}, \quad \forall \omega \in \Omega.$$

$$(36)$$

Constraints (28) and (29) indicate the UAV operator must either cancel the mission or select a feasible path and continue the current mission for the first and second periods, respectively. Constraints (30), (31), and (32) define the selected paths and their distances during each period, while constraint (33) defines the traveling distance when the operator decides to cancel the mission in the second period, and direct it to the origin. Constraint (34) ensures that two consecutive paths are connected by a common waypoint, while constraint (35) defines binary variables.

Given this formulation, it can be noted that the objective (27) function is a nonlinear function of the decision variables, as it involves products of two variables. In addition, energy consumption constraints (18) and (20) include nonlinear functions of speed variables, and battery constraint (21) involves the max operator. In the following subsection, we address these nonlinearities and propose a tight linear approximation for the objective function and the nonlinear constraints so that the underlying optimization problem can be modeled as a linear integer programming problem.

4.2. Model linearization

In this section, we develop a linear reformulation of the proposed model through a series of steps that involve linearization of the nonlinear objective (27) and constraints (18), (20), and (21). We first discuss the linearization of the objective function, and then discuss the nonlinear constraints.

4.2.1. Linearization of the objective function

The objective function (27) involves two types of nonlinearity. First, $cost_{tot}(N_{2,s}^{\omega})$ is a nonlinear function due to the max operator used in the calculation of the mission delay cost $C_{delay}(N_{2,s})$ as indicated in Eq. (6). In addition, the objective contains products of two variables in the terms $(1-Y_1) \cdot cost_{tot}(N_{1,2})$, $Y_2^{\omega} \cdot cost_{tot}(N_{2,o}^{\omega})$, and $(1-Y_1-Y_2^{\omega}) \cdot cost_{tot}(N_{2,s}^{\omega})$. To this end, we first introduce a new variable $\Gamma_{2,s}$ and the following constraints to linearize $cost_{tot}(N_{2,o}^{\omega})$:

$$C_{delay}(N_{2,s}) = c_W \cdot \Gamma_{2,s} \tag{37}$$

$$\Gamma_{2,s} \ge l_r + \frac{\sum_{\omega \in \Omega} p_\omega \cdot N_{2,s}^\omega}{\bar{p}} - \Delta_e \tag{38}$$

$$\Gamma_{2,s} \in \mathbb{R}^+$$
. (39)

Once this transformation is performed, we introduce three more sets of variables, i.e., $\Lambda_{1,2}$, $\Lambda_{2,o}^{\omega}$ and $\Lambda_{2,s}^{\omega}$, and also the following constraints to linearize the bilinear terms:

$$A_{1,2} \le M \cdot (1 - Y_1) \tag{40}$$

$$\Lambda_{1,2} \ge cost_{tot}(N_{1,2}) - M \cdot Y_1 \tag{41}$$

$$\Lambda_{2a}^{\omega} \le M \cdot Y_{2a}^{\omega}, \quad \forall \omega \in \Omega$$
 (42)

$$\Lambda_{2a}^{\omega} \ge cost_{tot}(N_{2a}^{\omega}) - M \cdot (1 - Y_{2}^{\omega}), \quad \forall \omega \in \Omega$$
 (43)

$$\Lambda_{2s}^{\omega} \le M \cdot (1 - Y_1 - Y_2^{\omega}), \quad \forall \omega \in \Omega$$
(44)

$$\Lambda_{2c}^{\omega} \ge cost_{tot}(N_{2c}^{\omega}) - M \cdot Y_{2c}^{\omega}, \quad \forall \omega \in \Omega$$
 (45)

$$\Lambda_{1,2}, \Lambda_{2,\alpha}^{\omega}, \Lambda_{2,\alpha}^{\omega} \in \mathcal{R}^+, \quad \forall \omega \in \Omega, \tag{46}$$

where M is a large positive constant that guarantees that we can always find feasible solutions for $\Lambda_{1,2}$, $\Lambda_{2,s}^{\omega}$ and $\Lambda_{2,o}^{\omega}$. With the above constraints, if the mission is cancelled at the beginning of the first period (i.e., $Y_1=1$), $\Lambda_{1,2}=0$; otherwise, $\Lambda_{1,2}=cost_{tot}(N_{1,2})$. Similarly, if the mission is cancelled at the beginning of the second period under scenario ω (i.e., $Y_2^{\omega}=1$), $\Lambda_{2,s}^{\omega}=0$ and $\Lambda_{2,o}^{\omega}=cost_{tot}(N_{2,o}^{\omega})$; otherwise, $\Lambda_{2,s}^{\omega}=cost_{tot}(N_{2,s}^{\omega})$ and $\Lambda_{2,o}^{\omega}=0$. Thus, it is equivalent to the original objective function to have the following linearized objective function, $\min Y_1 \cdot cost_{tot}(N_{1,o}) + \Lambda_{1,2} + \sum_{\omega \in \Omega} p_{\omega} \{\Lambda_{2,o}^{\omega} + \Lambda_{2,s}^{\omega}\}$, with the above constraints used to define the linear terms.

4.2.2. Linearization of the nonlinear constraints

As noted above, nonlinearities exist in two distinct sets of constraints. We address these separately in the following paragraphs: Energy Consumption Constraints (18) and (20): The energy consumption constraints are nonlinear due to the inclusion of function $P_{hor}(V_{i,j})$, which is a nonlinear convex function with respect to flight speed $V_{i,j}$. Thus, we linearize $P_{hor}(V_{i,j})$ via a set of tangent lines as follows. Consider that $V_{i,j}$ is within the interval $[0,v_{max}]$ with M+1 breakpoints, i.e $v_0=0 < v_1 < \cdots < v_M = v_{max}$. Then the tangent line of function $P_{hor}(V_{i,j})$ at point $(v_m, P_{hor}(v_m))$, $m=0,1,\ldots,M-1$ can be expressed as: $P_m(V_{i,j})=P'_{hor}(v_m)\cdot (V_{i,j}-v_m)+P_{hor}(v_m)$, where $P'_{hor}(v_m)$ represents the derivative of $P_{hor}(V_{i,j})$ at point $(v_m, P_{hor}(v_m))$. In addition, as our objective function is to minimize energy consumption, it is sufficient to have the following inequality constraints. Therefore, the nonlinear constraints (18) and (20) can be linearized as:

$$E_{1,2} \ge P_m(V_{1,2}) \cdot I_r, \quad \forall m \in \{0, \dots, M\}$$
(47)

$$E_{2,s}^{\omega} \ge P_m(V_{2,3}^{\omega}) \cdot l_l + P_{hor}(\bar{v}) \cdot \frac{N_{3,s}^{\omega}}{\bar{v}}, \quad \forall m \in \{0, \dots, M\}, \omega \in \Omega.$$
(48)

Battery Capacity Constraints (21): The nonlinear battery constraints can be linearized by the following constraints involving the dummy variables $E_1 = \max(P_{hor}(\bar{v}) \cdot \frac{N_{1,o}}{\bar{v}}, E_{1,2})$ and $E_2^\omega = \max(E_{2,o}^\omega, E_{2,s}^\omega)$. This is again due to the minimization of the energy consumption costs in the objective function:

$$E_1 + E_2^{\omega} \le \eta \cdot Cap_e^B, \quad \forall \omega \in \Omega$$
 (49)

$$E_1 \ge P_{hor}(\bar{v}) \cdot \frac{N_{1,o}}{\bar{v}} \tag{50}$$

$$E_1 \ge E_1 \,, \tag{51}$$

$$E_{2}^{\omega} \ge E_{2\alpha}^{\omega}, \quad \forall \omega \in \Omega$$
 (52)

$$E_2^{\omega} \ge E_{2,s}^{\omega}, \quad \forall \omega \in \Omega.$$
 (53)

Based on the above transformations, the updated linear stochastic programming model is denoted as follows:

$$\min Y_1 \cdot cost_{tot}(N_{1,o}) + \Lambda_{1,2} + \sum_{\omega \in \mathcal{O}} p_{\omega} \{\Lambda_{2,o}^{\omega} + \Lambda_{2,s}^{\omega}\}$$

s.t. Constraints (13)-(17), (19), (22), (25), (28)-(53).

4.3. Weather scenario generation using probabilistic weather forecasts

The stochastic programming models developed in Sections 4.1 and 4.2 assume the availability of scenario-based weather forecasts. A representative of such forecasts is ensemble forecasting (Leutbecher and Palmer, 2008). Instead of providing a single forecast, ensemble weather forecasting provides a set of weather predictions that indicate the range of possible future states of the atmosphere. These ensemble members are typically obtained by slightly altering initial conditions/parameters that model the atmospheric physical processes and then running forecast models a number of times (Arribas et al., 2005; Lu et al., 2007). It has been noted that ensemble forecasting is an effective way to quantify weather prediction uncertainty by capturing the spread of the solutions in the ensemble, which brackets the true weather outcome (Steiner et al., 2008). Based on Ren et al. (2007), we propose a weather scenario generation algorithm based on ensemble forecasts in this section. More specifically, rather than using the ensemble forecasts directly, our weather scenario generation algorithm performs a mapping from weather forecast information to realizations of possible weather blockage maps, including a simulation of ensemble weather and a conversion from ensemble weather to cell blockage maps.

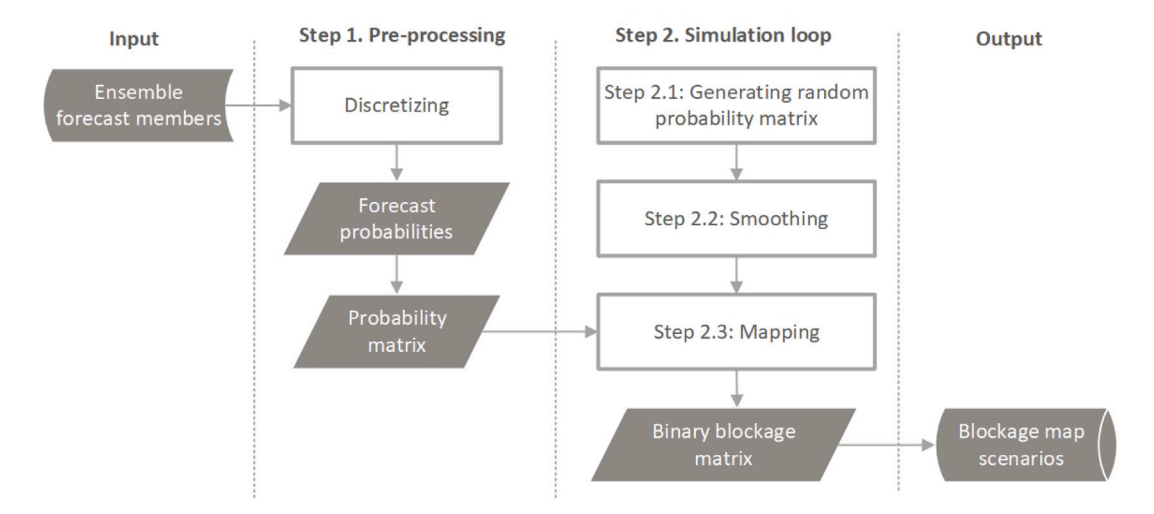


Fig. 4. An overview of the weather scenario generation algorithm.

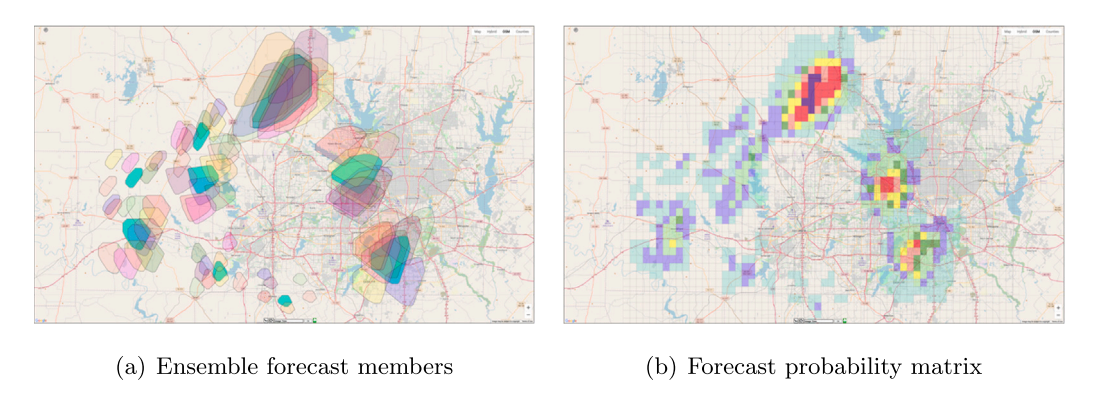


Fig. 5. Step 1. Pre-processing: Generating probability matrix from ensemble forecast members (In Fig. 5(a), each set of polygons with the same color denotes one weather ensemble forecast member; in Fig. 5(b), the lighter the color of a cell (i, j), the lower the probability $p_{i,j}$ that the cell will be blocked, e.g., light blue indicates $p_{i,j} = 0.1$, dark purple indicates $p_{i,j} = 1$). (For interpretation of the references to color in this figure legend, the reader is referred to the web version of this article.)

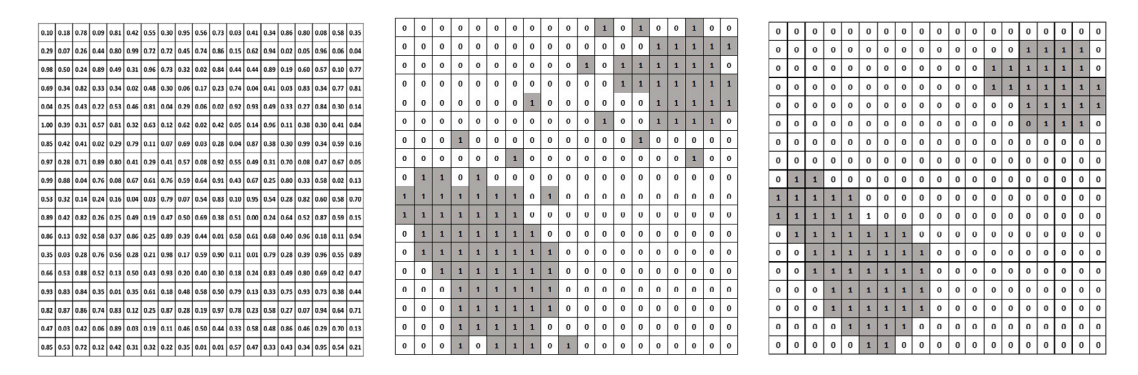
A diagram of the weather scenario generation algorithm is shown in Fig. 4, where gray rhomboids indicate input and output data, and the white rectangular boxes indicate the data processing steps we use to create the cell blockage map. The details of the algorithm are as follows:

Input: The input to the scenario generation algorithm includes initial ensemble forecast members for the atmosphere over the service region during the second period. The algorithm takes these forecast members into account to make predictions. Fig. 5 presents an example of an ensemble weather forecast, illustrating 10 forecast members in the left panel. Each member in the figure is represented by a set of polygons with the same color, indicating the airspace that will be affected by severe weather conditions (e.g., aviation disrupting convection) during the second period.

Step 1: After obtaining the ensemble members, the first step is to discretize each member onto the two-dimensional grid that represents the service region. Subsequently, the forecast probability of each grid cell (i, j) being blocked during the second period, i.e., $p_{i,j}$, is calculated. To do so, we calculate the ratio of ensemble members that indicate a blockage for a given cell, and obtain its blockage frequency. This information is then used to create a grid-based forecast probability matrix over the entire region. An example of a forecast probability matrix created based on 10 ensemble members is shown in the right panel of Fig. 5, where different colors represent different values of forecast probabilities.

Step 2: Once the forecast probability matrix is obtained, a sampling-based simulation is applied to map the matrix into a set of binary cell blockage maps:

Step 2.1: In each iteration, the initial step is to generate a random probability matrix that corresponds to the service region grid structure. This matrix consists of elements that are random numbers derived from a uniform distribution within the [0,1] interval, as depicted by the left-hand map in Fig. 6. Let $[u_{i,j}^{\omega}]_{I\times J}$ denote the random probability 2D matrix for scenario ω .



(a) Step 2.1 Random probability (b) Step 2.2 Binary blockage map (c) Step 2.3 Final blockage map matrix

Fig. 6. Step 2. Mapping from a probability matrix to cell blockage maps: Simple random sampling followed by smoothing.

Step 2.2: Following the generation of the random probability matrix, it is then mapped to an associated binary cell blockage map. A sample binary blockage map can be derived from the random probability matrix using the following formula:

$$b_{i,j,l}^{\omega} = \begin{cases} 1 & u_{i,j}^{\omega} \le p_{i,j} \\ 0 & \text{otherwise.} \end{cases}$$

For each element $u_{i,j}^{\omega}$ in the random probability matrix corresponding to cell (i,j), we perform a comparison with the forecasted probability of the same cell, denoted as $p_{i,j}$. If $u_{i,j}^{\omega} \leq p_{i,j}$, the corresponding cell (i,j) is to be blocked during the second period under that scenario, and $b_{i,j,l}^{\omega} = 1$; otherwise, a cell will not be blocked and $b_{i,j,l}^{\omega} = 0$. An example of the binary blockage map is shown in the center map of Fig. 6.

Step 2.3: Given the absence of spatial correlation or clustering of blocked cells in the blockage map generated in Step 2.2, we employ Gaussian smoothing technology to refine the map (Clarke et al., 2013). Following the smoothing process, the finalized blockage map, demonstrated in the right map of Fig. 6, is subsequently saved as output.

Output: Through the repetition of the previously described random sampling process, a collection of weather forecast scenarios, denoted as Ω , is created and utilized as input for the stochastic programming model. During this random sampling process, every scenario is independently generated, without any intrinsic bias towards or preference for a specific scenario. Consequently, all scenarios are assumed to have an equal likelihood of occurrence, denoted as $p_{\omega} = \frac{1}{|\Omega|}$.

Note that cell blockage maps generated in this way can closely approximate the blockage probabilities given by the original forecast probability matrix $[p_{i,j}]_{I \times J}$, while the blocked cells are clustered. We demonstrate the accuracy of our weather scenario generation algorithm in Appendix S3 through a comparison study between the data sets generated by the algorithm and the actual weather data. The comparison study also suggests that, as the number of generated weather scenarios increases, the percentage of instances where a cell is blocked at a specific time, based on the generated data sets, converges towards the actual forecast probability for that cell at that time interval.

5. Path planning in 3D environments

While we have proposed a general stochastic path planning method that can be effectively applied to 2D environments for various UAV missions, we recognize that UAV may need to make vertical adjustments during a mission to avoid obstacles or environmental conditions. To fulfill the above needs, we extend the proposed stochastic path planning method from 2D to 3D in this section. To do so, we now allow a UAV to fly vertically as needed, besides horizontal movements. In practical UAV implementations (Mag, 2020; Bell, 2021b), UAV movements are typically performed in either vertical or horizontal directions, rather than diagonal ones. Following these practical implementations, we do not consider simultaneous horizontal and vertical movements in our formulation. At the beginning of each period, the UAV operator first determines whether or not to cancel the current mission as described in Section 3.1. After that, s/he is able further to choose the UAV flight altitude of a mission. Let h_0 denote the original altitude that the UAV flies at before the current iteration, and let h_t indicate the altitude that the UAV flies at during period $t \in \{1,2\}$. As part of these altitude decisions, the operator can direct the UAV to ascend (descend) vertically at a constant speed \bar{v}_{ver} from the current altitude h_{t-1} to a higher (lower) altitude h_t . Note that if the UAV is to ascend, $h_t > h_{t-1}$; if the UAV is to descend, $h_t < h_{t-1}$. In addition, the operator can keep the flight at the current altitude, where $h_t = h_{t-1}$. After the decisions related to vertical movements, the UAV operator continues to make horizontal path planning decisions as described in Section 3.1 and operate the UAV correspondingly.

In order to accommodate the vertical movement, we adjust the cost functions as follows:

Economic costs for vertical movement: The energy usage cost $cost_{eco}(h_t)$ when a UAV flies vertically to achieve adjusted altitude h_t at flight speed \bar{v}_{ver} during period t is calculated based on the total energy consumption and the unit electricity price c_{EN} (Aiello et al., 2021):

$$cost_{eco}(h_t) = c_{EN} \frac{E_{ver}(h_t)}{n}, \tag{54}$$

where $E_{ver}(h_t)$ denotes the theoretical energy consumption when the UAV flies vertically, defined as:

$$E_{ver}(h_t) = \begin{cases} P_{asc,t} \cdot \frac{h_t - h_{t-1}}{\bar{v}_{ver}}, & h_t \ge h_{t-1}, \\ P_{dec,t} \cdot \frac{h_{t-1} - h_t}{\bar{v}_{ver}}, & h_t \le h_{t-1}. \end{cases}$$
(55)

Note that $\frac{h_t - h_{t-1}}{\bar{v}_{ver}}$ ($\frac{h_{t-1} - h_t}{\bar{v}_{ver}}$) represents the duration of ascending (descending) movement during period t. Moreover, the required power for ascending and descending during period t is determined as (Citroni et al., 2019):

$$P_{A,t} = \frac{1}{2}c_D s_f \rho_h (\bar{v}_{ver} + v_{A,t}^{wd})^3 \pm (m_0 + m_p)g v_{A,t}^a, \tag{56}$$

where $A \in \{asc, des\}$, asc and des indicate ascending and descending, respectively; \bar{v}_{ver} is flight speed and $v_{A,t}^{wd}$ is wind speed during period t.

It is important to note that current regulations limit UAVs to flying at low altitudes below 400 ft (FAA, 2023). At this altitude, changes in air density due to altitude adjustments are negligible. In fact, based on our numerical analysis, we found that a vertical adjustment of the UAV from 200 ft to 400 ft would only result in a slight change in air density of 0.8%. This, in turn, would have a negligible impact of less than 0.5% on the total expected cost of a UAV mission. Consequently, in our model, we have assumed a constant air density to simplify all involved calculations.

Environmental costs for vertical movement: The emission-related cost due to vertical movement to achieve adjusted altitude h_t , denoted as $cost_{env}(h_t)$, is calculated according to the unit cost of CO_2 emissions c_{EM} and the amount of CO_2 emitted for power generation, such that:

$$cost_{env}(h_t) = c_{EM} \xi_{grid} \frac{E_{ver}(h_t)}{\eta \cdot \eta_{\sigma}},$$
(57)

where ξ_{grid} is the CO₂ marginal emission rate which measures the CO₂ emitted at power generation facilities per kWh consumed by a UAV (Goodchild and Toy, 2018). On the other hand, $\frac{E_{ver}(h_t)}{\eta_{rg}}$ calculates the amount of electricity that needs to be generated at the power facilities for a UAV to receive usable electricity from the UAV battery, where η is the combined efficiency of battery charging and discharging, and η_r is the efficiency of transmission and distribution on the grid (Stolaroff et al., 2018).

We also notice that vertical movements during a mission take much less time compared to horizontal movements. For instance, launching and landing are the longest vertical movements, taking about ten seconds, whereas horizontal movements can take a number of minutes or even hours. As such, we disregard the impacts incurred by the time required for vertical movement when calculating the energy consumption for horizontal movement during each period. And further assume that the durations of horizontal movement during periods 1 and 2 are l_r and l_l , respectively, while the theoretical energy consumption when the UAV flies horizontally along the selected path during each period is calculated as $E_{1,2} = P_{hor}(V_{1,2}) \cdot l_r$ and $E_{2,3} = P_{hor}(V_{2,3}) \cdot l_l$, respectively.

Based on the above notations, the total cost when a UAV flies vertically to achieve altitude h_t can be denoted as $cost_{tot}(h_t) = cost_{eco}(h_t) + cost_{env}(h_t)$. Then the stochastic programming model to identify an initial path that minimizes the total expected cost of the flight over the first period of each iteration can be expressed as follows:

$$\min Y_{1} \cdot \{ cost_{tot}(h_{1}) + cost_{tot}(N_{1,o}) \} + (1 - Y_{1}) \cdot \{ cost_{tot}(h_{1}) + cost_{tot}(N_{1,2}) \} + \sum_{\omega \in \Omega} p_{\omega} \{ Y_{2}^{\omega} \cdot \{ cost_{tot}(h_{2}^{\omega}) + cost_{tot}(N_{2,o}^{\omega}) \} + (1 - Y_{1} - Y_{2}^{\omega}) \cdot \{ cost_{tot}(h_{2}^{\omega}) + cost_{tot}(N_{2,s}^{\omega}) \} \}$$

$$(58)$$

s.t. Constraints (10)-(26)

$$h_1 \in [h, \overline{h}] \tag{59}$$

$$h_2^{\omega} \in [h, \overline{h}], \quad \forall \omega \in \Omega.$$
 (60)

Compared to the objective Eq. (27) in the 2D model, the new objective Eq. (58) in the 3D model also includes the costs due to vertical movements, $cost_{tot}(h_1)$ and $cost_{tot}(h_2^{\omega})$. Constraints (59) and (60) guarantee that the UAV always operates within a safe and suitable altitude range, where \underline{h} represents the lower bound and \overline{h} represents the upper bound of the allowable flight altitude. For instance, regulations for small UAVs limit their altitude to 400 ft (FAA, 2020). Moreover, in some cases, UAVs must fly above a specific altitude to avoid obstacles such as trees or buildings.

6. Numerical analysis

In this section, we conduct a series of numerical analyses using computer simulations to evaluate the performance of our proposed approach above and to obtain practical insights for UAV delivery services. Implementing our method requires inputting

Table 2
UAV types and typical use cases (Porsche Consulting, 2018).

Types	Typical use cases		Model examples
Parcel	Last-mile express delivery Delivery network extension	Cargo transportation Emergency transport	Wing, Apt70
Passenger	· Aircraft rental · Air bus	Rescue operations On-demand air taxi	eCRM-003, Voyager
Inspection	Inspection and monitoring Surveying and mapping	Precision agriculture/farming Media and entertainment	DJI Mini

Table 3
Technical parameters.

Notation	Description	Unit	DJI Mini	Wing	Apt70	eCRM-003	Voyager
m_0	UAV mass	lb	0.6	11.4	300	4000	1235
m_p	Payload mass	1b	N/A	2.6	70	980	440
s_f	UAV front surface	m^2	0.006	0.5	3	10	6
c_D	Aerodynamic drag coefficient	-	0.8	1.4	1.5	1	1.2
Cap^{B}	Battery capacity	kWh	0.03	10	57	600	140
Range	UAV flight range	mi	15.5	12	35	60	25
v_{max}	Maximum UAV ground speed	mph	36	64.9	127	200	81
\bar{v}	Expected UAV speed	mph	22	43	67	150	52

UAV specifications, weather data, and related cost and other parameters. UAV specifications and cost parameters can be obtained from existing literature and reports, while live weather information and ensemble forecasts for the service region can be acquired from the Collaborative Adaptive Sensing of the Atmosphere (CASA) radar network (CASA, 2020; Radhakrishnan and Chandrasekar, 2020). Further details on input data are provided in Section 6.1.

Once the input data is available, we initially apply our weather scenario generation algorithm to produce a set of weather scenarios derived from ensemble weather forecasts. Additionally, we have created a user-friendly website tool (CASA, 2022), capable of reading generated weather scenarios and simulating path-planning procedures for a given mission and UAV specifications. To facilitate real-world applications, our website tool enables users to input simulation parameters, including origin, destination, and mission types. Subsequently, it can generate and visually represent all possible paths for each mission, highlighting the optimal paths and their associated waypoints as per our proposed approach.

To execute the optimal path, the UAV operator should guide the UAV to fly from its current position to the selected waypoint along the optimal path. As the UAV approaches a waypoint, the UAV operator can repeat the aforementioned processes to obtain an updated path and waypoints until reaching the destination.

6.1. Experimental setup

6.1.1. UAV specifications

The study conducted by Porsche Consulting (2018) classifies UAVs into three distinct segments based on their intended purposes, namely parcel, passenger, and inspection UAVs. Parcel UAVs are designed to deliver time-sensitive goods, while passenger UAVs cater to intracity and intercity transportation requirements. Inspection UAVs, on the other hand, aid in monitoring and surveying infrastructure or covering events. Additionally, parcel and inspection UAVs are generally small, while passenger UAVs are usually larger. We have followed the above categorization framework and provided the associated typical use cases for each category in Table 2. In addition, we have chosen 1–2 UAV models for each category as examples and listed their specifications in Table 2 (DJI, 2023; Wing, 2023; Bell, 2021a; EVTOL, 2021; Uber Elevate, 2021; Holden and Goel, 2016; Uber Elevate, 2023). While our proposed stochastic path planning method can be applied to various types of UAVs and use cases, our simulations primarily focus on parcel and passenger UAVs. Note that one main objective of this study is to demonstrate the effectiveness of our proposed stochastic method in uncertain weather conditions. However, inspection UAVs are typically used for monitoring and inspection missions with short distances or short durations in deterministic weather conditions, which makes them unsuitable for demonstrating our proposed stochastic method. Therefore, we have excluded inspection UAVs from our simulation.

For parcel and passenger UAVs, we then pick a specific model and consider a corresponding use case, respectively. The model selected for parcel delivery is Autonomous Pod Transport 70 (APT-70), designed by Bell. The technical parameters of this model are shown in Table 3 based on existing descriptions and documents (Bell, 2021a; EVTOL, 2021). Specifically, APT-70 is an electric vertical takeoff and landing cargo UAV developed for commercial and military use. It has unique features such as bi-plane wings, vertical thrust modules, no central fuselage, tail-sitter-styled landing gear, and a modular design for easy storage and transportation. Notably, the APT-70 has a gross weight of 300 lbs and can carry a payload of up to 70 lbs. It is powered by batteries with a capacity of about 57 kWh, which enables a range of about 35 miles and a maximum speed of up to 127 mph. For the use case of APT-70, we consider a parcel transportation service within its flight range limit.

In terms of passenger UAVs, we consider a standard reference model created by Uber, called eCRM-003. The parameters of eCRM-003 are listed in Table 3 as obtained from Uber Elevate (2021) and an Uber white paper (Holden and Goel, 2016). For the

use case of passenger UAVs, we consider a city-to-city commute service, assuming that each mission transports four passengers and one pilot. It is worth noting that the eCRM-003 has a gross weight of 4000 lbs and a payload weight of 980 lbs, which includes one pilot, four passengers, and their luggage. Like the APT-70, it is powered by batteries, but with a larger capacity of 600 kWh. This enables a flight range of approximately 60 miles and a maximum speed of up to 200 mph.

For demonstration purposes, both types of UAVs are assumed to fulfill delivery demand within Dallas-Fort Worth Metropolitan Area (DFW), delivering parcels and passengers from an origin to a destination, respectively. The service region of DFW is then divided into a two-dimensional grid (X,Y) in Cartesian coordinates with 50 rows and 60 columns, as shown in Fig. 5(b). For our analysis, the origin and destination of a mission are randomly picked within this area, where the flight distance does not exceed the maximum range of the UAV.

6.1.2. Weather data

For both use cases, the information on live weather and ensemble forecasts in the service region is produced by the modified CASA nowcasting algorithm (Radhakrishnan and Chandrasekar, 2020). This algorithm is run operationally for the DFW metroplex in North Texas (TX) and is able to produce high-resolution gridded ensemble forecast members, with forecasts of radar reflectivity in one-minute intervals out to 20 min into the future. In this study, we use the above algorithm to generate 10 ensemble members for the airspace within our service region every five minutes. Thereafter, we apply a contouring algorithm to those ensemble member grids, deriving geofenced regions of significant precipitation to use as obstacles for avoidance in each scenario (Maple, 2003). Based on the above information, we assume the duration of each period to be 5 min. For demonstration purposes, we directly use the 10 ensemble members as weather scenarios to capture the stochastic weather evolution. If additional scenarios are required, we can utilize these members and apply the weather scenario generation algorithm described in Section 4.3. In particular, each member is initially discretized into a 50 by 60 two-dimensional grid, which corresponds to the service region discretization in the DFW area. Subsequently, we compute the forecast probability of each cell being obstructed. We then implement Step 2 of the weather scenario generation algorithm, which generates a set of binary cell blockage maps based on the resulting forecast probability matrix.

6.1.3. Cost and other parameters

As part of other input parameters, the unit electricity price is assumed to be \$0.1331 per kWh based on the average price a customer in the U.S. pays for electricity (Electric Choice, 2021). To calculate the actual energy usage costs and emission costs, we set the combined efficiency of battery charging and discharging to be 85% (Goodchild and Toy, 2018), and set the efficiency of power transmission and distribution equal to 95% (EPA, 2021a). The unit cost of CO₂ emissions equals 0.009 \$/lb, which is based on the CO₂ emission trading market in the U.S. (World Bank, 2021). According to the U.S. Environmental Protection Agency's latest available data (EPA, 2021b), the CO₂ marginal emission rate is assumed to be 0.709 kg/kWh. The mission cancellation cost of parcel delivery is set to be 106% of the unit profit on that item, which is based on an analysis by Zohar (2018) involving order decline rates, direct profit loss, and their potential implications for a retailer. When it comes to the mission cancellation cost of commute services, we set it equal to \$154.4 per mission estimated by the average cost of canceling a commercial scheduled flight (Eurocontrol, 2020), which considers loss of revenue, loss of future value, passenger care and compensation costs and so on. In defining the base level of unit noise cost for passenger UAVs, we use the estimate of Van Essen et al. (2019) who suggest an average noise cost of \$0.035 per mile traveled for short-haul flights. For parcel UAVs, we consider factors such as actual take-off weight, flight speed, and flight altitude and calculate the noise level incurred by operations of both types of UAVs, then proportionally approximate the unit noise cost of parcel UAVs based on the benchmark value for passenger UAVs (Gagliardi et al., 2018).

As described in Section 3.2, we calculate the planned mission completion time of each mission via the distance between the origin and destination divided by the expected UAV speed. The expected UAV speed of parcel delivery missions is set to 67 mph, while it is 150 mph for passenger delivery missions, as shown in Table 3. If a parcel delivery mission is delayed beyond its planned mission completion time, we assume that a delay cost of \$0.5/h is incurred to be calculated according to the duration of the delay. This cost is estimated based on Allon et al. (2011) by considering how sales volumes depend on pricing and waiting times, where the conclusion is that consumers attribute an implicit cost to the waiting time that amounts to many times the average wage. In terms of passenger commute services, if a mission of commute services is delayed beyond its planned mission completion time, we assume a delay cost of \$474/h in line with the average delay cost of U.S. commercial airlines. This cost is calculated based on a case study by Ferguson et al. (2013), where the authors examine delay costs for U.S. airline departures from 12 major airports. In the following sections, we have also performed detailed sensitivity analyses around these baseline values to study how they will affect decisions and expected costs.

6.2. Path establishment

In this section, we demonstrate how we implement the two-stage stochastic programming model in a rolling horizon manner to establish the optimal initial path during each iteration so that the UAV is able to fly from a given origin to a given destination based on the periodically updated weather forecast information. As described in Section 3, an iteration consists of two periods, each lasting 5 min. Note that the operator has perfect weather information for the first period and has an available probabilistic weather forecast for the second period. In addition, the objective of each iteration is to identify the optimal initial path along which the UAV can fly during the first period based on the current observed weather and available weather forecasts.

For demonstration purposes, we take a passenger delivery mission as an example in Fig. 7, randomly define a location in Arlington, TX as the origin of the passenger delivery mission (marked as a circle), and define a location in Forney, TX as the

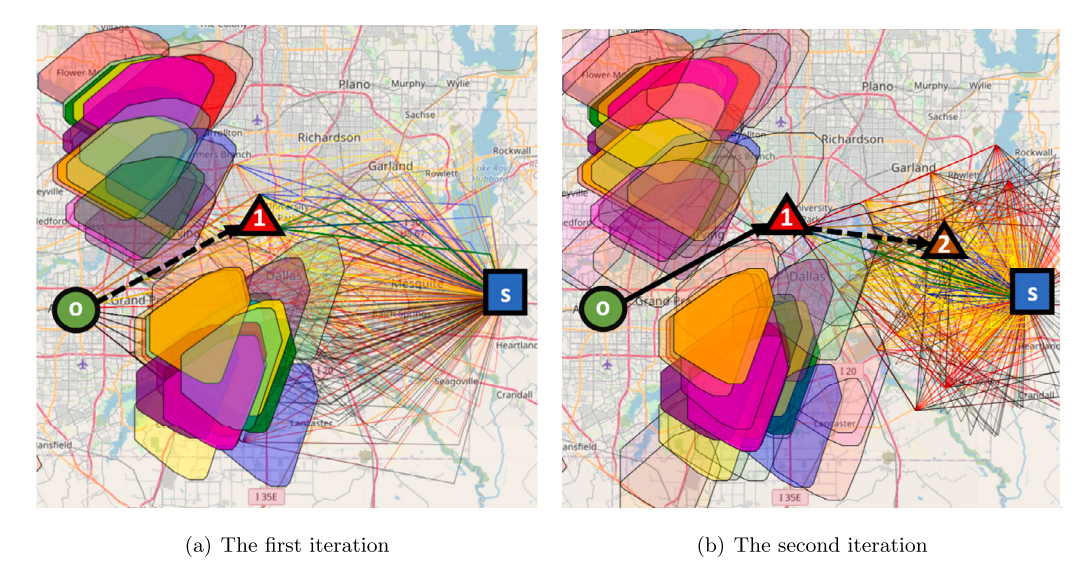


Fig. 7. Path establishment and update in the first iteration and the second iteration, respectively. (For interpretation of the references to color in this figure legend, the reader is referred to the web version of this article.)

destination of the mission (marked as a square). The Euclidean distance between the origin and destination is 36.9 miles, which corresponds approximately to 14 min of travel time based on the average flight speed for passenger delivery missions. As the duration of one period in each iteration lasts 5 min, it requires three iterations to generate feasible paths from origin to destination along which the UAV can fly, whereas the third iteration only consists of one single period, given there are only 4 min left. Thus, our demonstration in Fig. 7 includes the two iterations of the mission, which shows how the potential paths are generated and how the optimal initial path among those candidates is chosen. Fig. 7 also contains the weather information used for each iteration: the blocked airspace due to severe weather conditions during the first period is denoted as polygons with deep colors, while the blocked airspace during the second period is indicated as polygons with light colors.

During the first iteration shown in Fig. 7(a), the proposed algorithm considers a set of potential waypoints around the origin and generates a potential path between the origin and each waypoint, which is established specifically for the first period. Furthermore, for each potential waypoint, the algorithm also generates a set of potential paths between that waypoint and the destination according to the available probabilistic weather forecast for the second period. The algorithm then searches among all potential waypoints and picks the best one that is able to detour around blocked airspace and incurs the lowest expected total cost. The chosen waypoint during the first iteration is marked as a triangle with "1" inside, as shown in Fig. 7(a). When the UAV flies along the corresponding initial path (marked as a dashed line), it is able to avoid entering the blocked airspace with severe weather conditions during the initial five minutes and arrive at the chosen waypoint. Immediately before the UAV arrives at the chosen waypoint 1, the algorithm starts the second iteration. As shown in Fig. 7(b), the algorithm considers a set of potential waypoints around waypoint 1 and generates a potential path between waypoint 1 and each potential waypoint. According to the same criteria, the algorithm then searches among all potential waypoints and picks the best one, marked as a triangle with "2". The UAV then flies along the chosen initial path, marked as a dashed line in Fig. 7(b), and arrives at waypoint 2. We also notice that the UAV is able to fly directly to the scheduled destination after two iterations as it flies away from the blocked airspace.

6.3. Optimal policies and sensitivity analysis on key parameters

In this section, we perform sensitivity tests over two different types of UAV use cases to investigate how the expected total cost varies with respect to key model parameters. Based on these experiments, we generate insights for UAV-based delivery services.

6.3.1. Expected total cost as a function of different cost parameters

We also explore how the expected total costs of the parcel and passenger delivery missions vary with respect to key cost parameters when our proposed method is implemented. More specifically, Figs. 8(a) and 8(b) show how expected total costs change in percentage when the value of a focal cost parameter varies with others being fixed. It can be observed in both figures that the expected total cost is more sensitive concerning the unit energy usage $\cot(c_{EN})$ compared to the unit cost of CO_2 emissions (c_{EM}) . Take the passenger delivery missions as an example, the expected total cost increases (decreases) by around 15% as the unit energy usage cost increases (decreases) by 25%. However, the expected total cost changes slightly as the unit cost of CO_2 emissions increases. Another observation is that the expected total cost is more sensitive to unit noise cost in parcel delivery missions than in passenger delivery missions. The expected total cost of parcel delivery missions decreases (increases) by around 11% as the unit noise cost decreases (increases) by 25%, while that of passenger delivery missions only changes 1%. The above results imply that,

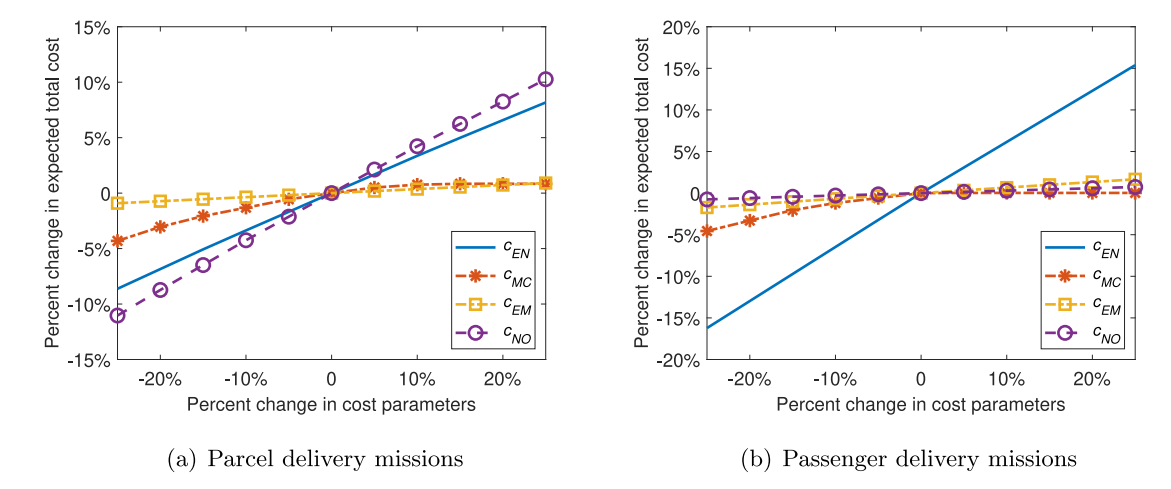


Fig. 8. Change in expected total cost over different model parameters (c_{EN} : unit energy usage cost; c_{MC} : fixed cancellation cost; c_{EM} : unit cost of CO₂ emissions; c_{NO} : unit noise cost).

in order to cut the expected total cost of both types of delivery missions, the decision maker should try to decrease the effective unit energy usage cost, unit cost of CO_2 emissions, or unit noise cost. More specifically, in order to reduce effective unit energy usage cost, the decision maker can potentially recharge more UAV batteries when the unit electricity price is at a low level, e.g., during early morning and late evening hours. The decision maker can also potentially adjust the flight height for different missions since the higher the altitude that UAVs fly at, the smaller the noise effect is. However, a trade-off analysis needs to be done between the decreased noise cost and the cost of flying at a higher altitude, as the latter incurs extra energy usage costs and emission-related costs.

We also observe that, for both use cases, the expected total cost changes significantly according to the unit mission cancellation cost, where it first increases and then keeps constant as the unit mission cancellation cost increases. The reason is that when the unit cost of canceling a mission is not so high, it can be a better option for a decision maker to cancel tasks that either face dramatically evolved weather conditions or require long UAV travel distances, as operating or continuing such types of missions will incur high operational costs. The increase in unit cancellation cost will thus contribute to an increased expected total cost. However, when the unit mission cancellation cost keeps increasing, the marginal cost of operating/continuing missions becomes lower than the marginal increase of cancellation cost, and the decision maker will cancel fewer missions. Thus, the impact of the unit mission cancellation cost on the expected total cost becomes less significant. When the unit mission cancellation cost becomes very large, the decision maker has to operate all missions to avoid the considerable cancellation penalty. Hence, the total cost curve keeps constant even if the unit cancellation cost increases. Based on the above observations, it can generally be concluded that a decision maker should try to decrease the unit cancellation costs to reduce the expected total cost. The decision maker should make good use of weather forecasts and potentially disable UAV services in the corresponding regions that will be affected by future severe weather conditions rather than accepting orders and then canceling them. In addition, the decision maker should also focus on missions with an appropriate traveling distance since long-distance missions lead to high operating costs, are more susceptible to weather conditions, and are thus more likely to be cancelled.

6.3.2. Expected total cost as a function of mission delay thresholds and costs

In this section, we further investigate how the expected total costs vary with respect to the planned completion time and the unit cost of mission delay when our proposed policies are implemented. As expected, the decision maker will bear lower expected total costs with lower unit mission delay costs and longer planned mission completion times. More specifically, we find in Fig. 9(a) that the expected total cost of parcel delivery missions decreases (increases) by around 2% as the planned completion time increases (decreases) by 25%. In addition, it increases (decreases) by around 2.5% when the cost of mission delay increases (decreases) by 25%. We also study the case of passenger delivery missions and observe similar trends in Fig. 9(b). Compared to parcel delivery missions, the expected total cost of passenger delivery missions is much more sensitive to the planned completion time. More specifically, the expected total cost of parcel delivery missions significantly increases by around 52% as the planned completion times decrease by 25%, while it decreases by 17% as the planned completion times increase by 25%. The difference is due to the high unit cost of mission delay set for passenger delivery missions compared with that of parcel delivery missions. As a result, even a slight decrease in the planned completion time would result in a massive increase in delay costs of passenger delivery missions.

The above results imply that, in order to decrease expected total costs, the decision maker should try to increase the effective planned completion time and/or reduce the effective unit cost of mission delay. As different customers may have different delivery time preferences and requirements, it would be desirable to offer a varying selection of planned completion times, which can reduce the overall effective planned completion time and, eventually, the cost of passenger delivery missions. The decision maker can also compensate customers with extra credit if they choose to wait longer, specifically for customers of passenger delivery missions.

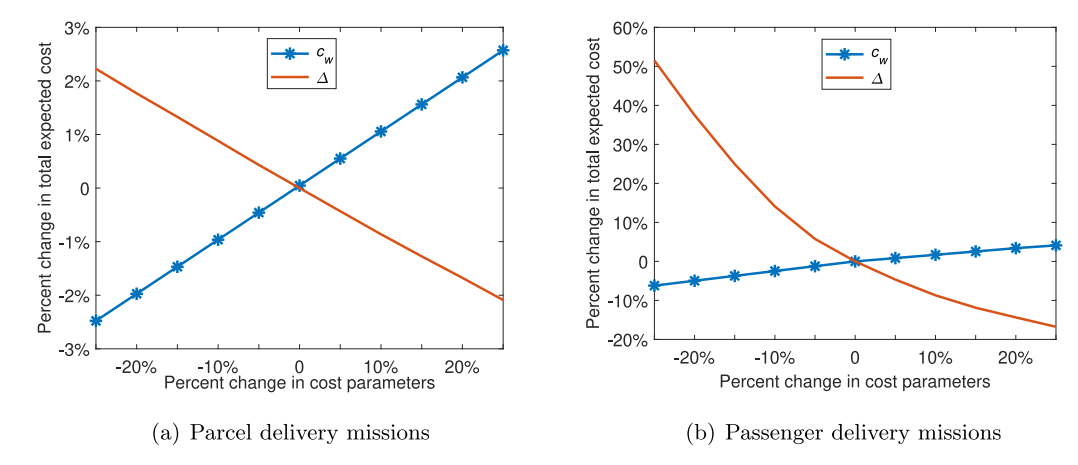


Fig. 9. Change in expected total cost over the unit cost of mission delay (c_W) and the planned completion times (Δ).

Table 4
Weather information and average savings due to stochastic method.

Weather condition index	Average savings (%)					
	Parcel delivery missions	Passenger delivery missions				
0.1	0.27%	0.26%				
0.2	1.83%	1.83%				
0.3	3.72%	4.24%				
0.4	6.30%	5.22%				
0.6	6.80%	7.08%				
0.7	8.47%	10.49%				
0.8	11.91%	11.38%				

However, a trade-off analysis needs to be done between the cost of offering extra credit and the decreased expected total cost. In addition, firms that offer UAV passenger delivery services shall carefully select the planned service completion time by considering its significant impact on the total operating cost.

6.4. Validation of proposed stochastic method

We validate the proposed stochastic approach using a real-world example, which includes weather information and UAV specifications, and compare the performance of our stochastic approach with deterministic path-planning methods that represent the current practice. To this end, we solve the UAV path planning problem via two methods: our proposed stochastic method and the deterministic version of our stochastic method that assumes all future weather scenarios are fixed as an expected value. Once we identify the optimal paths under the two methods, we calculate the expected total cost of flying each path using the objective function (27) over the same set of random weather scenarios. Subsequently, we calculate the gap between these two expected total costs, which represents the savings achieved by implementing the stochastic solution. Additionally, we investigate the impact of variance in the stochastic weather information on the stochastic solution to further evaluate the performance and effectiveness of the approach in diverse scenarios and its capability to handle uncertain and dynamic conditions.

As part of our analysis, we introduce a weather condition index as a measurement of the severity and complexity of random weather conditions. We calculate the weather condition index as follows. Given a mission, we generate a large number of potential paths between the origin and destination to represent all such possible paths. Similar to the path generation in Section 4.1, we consider a set of potential waypoints around the origin and establish paths between each potential waypoint and the origin/destination, regardless of the weather conditions and the corresponding blocked airspace. For each potential path between the origin and destination, we count how many blocked airspaces it intersects in each scenario, and then obtain the total number of such intersections over all the scenarios. Note that the number of blocked airspaces in each scenario may vary. Once we have this total number of intersected blocked airspaces over all scenarios, we divide this sum by the total number of paths to get an average number of intersections per path. To ensure that we have a standardized measure in the range of [0,1], we divide this average number by the total number of blocked airspaces across all the scenarios to obtain the weather condition index for that mission. The larger the weather condition index, the more variant and disruptive the weather condition is for a given mission.

To validate our proposed stochastic method, we randomly select 30 different pairs of locations within the Dallas-Fort Worth Metropolitan Area as origins and destinations of missions for the two use cases as described in Section 6.1.1. We then recategorize 30 missions in each use case into seven groups based on the value of their real data-based weather condition indexes and calculate the average savings achieved by implementing the stochastic approach for each group, as shown in Table 4. The results indicate

Table 5Expected total potential costs and average travel distance by objective weights and mission type over 30 randomly picked missions.

Weights	Parcel delivery missions				Passenger delivery missions					
	Econ (\$)	Envi (\$)	Soci (\$)	Total (\$)	Dist (mile)	Econ (\$)	Envi (\$)	Soci (\$)	Total (\$)	Dist (mile)
(1,0,0)	41.76	3.44	20.67	65.87	37.85	1168.50	94.98	33.65	1297.13	37.67
(0,1,0)	44.73	3.24	21.18	69.15	38.61	1844.50	59.02	34.35	1937.87	38.38
(0,0,1)	46.32	3.34	14.97	64.63	39.34	1842.20	66.89	23.96	1933.05	39.25
$(\frac{1}{3}, \frac{1}{3}, \frac{1}{3})$	42.23	3.47	15.37	61.07	37.89	1172.90	91.31	27.90	1292.11	37.82
$(\frac{1}{2},0,\frac{1}{2})$	45.65	3.32	15.19	64.16	38.48	1691.40	65.93	24.82	1782.15	38.40
$(\frac{1}{2}, \frac{1}{2}, 0)$	45.31	3.28	15.67	64.26	38.52	1700.70	65.62	24.86	1791.18	38.47
$(0,\frac{1}{2},\frac{1}{2})$	45.95	3.30	15.07	64.32	38.92	1726.60	65.74	24.18	1816.52	38.76
$(\frac{2}{4}, \frac{1}{4}, \frac{1}{4})$	45.35	3.29	15.14	63.78	38.46	1680.00	65.68	24.68	1770.36	38.48
$(\frac{1}{4}, \frac{2}{4}, \frac{1}{4})$	45.46	3.27	15.20	63.93	38.55	1687.50	65.63	24.80	1777.93	38.52
$(\frac{1}{4}, \frac{1}{4}, \frac{2}{4})$	45.66	3.29	15.07	64.02	38.61	1711.20	65.70	24.58	1801.48	38.53

that the average savings of implementing our stochastic method are around 6% under both use cases, demonstrating the value and effectiveness of the stochastic method. Another observation is that the average savings increase as the weather index increases, which holds for both use cases. More specifically, we find that the average saving is minimal when the weather index is small. For example, the average savings of both cases is as low as 1.8% when the weather index is below 0.2. The average savings become significant as the weather index increases to high levels, rising to around 12% for both cases when the weather index increases to 0.8. In addition to the robustness of our proposed approach, this also suggests that the decision maker may use deterministic methods to identify a path when weather conditions are not so severe and complex, but shall implement a stochastic method when the weather conditions evolve more and more dramatically.

6.5. Impact of objective priority

In this section, we investigate how different objectives in UAV path planning may affect the expected total costs. As described in Section 3.2, we categorize all relevant costs incurred into three different types: economic, environmental, and social costs. As part of our analysis, we plan the optimal paths for 30 randomly picked missions based on ten different combinations of objective weights. We then compare the potential expected total costs achieved through the optimal paths in each case as shown in Table 5 based on simulation results. The first columns in Table 5 list the specifics of each weight combination over the three types of costs. In particular, the first, second, and third values of each combination signify the weight accorded to economic, environmental, and social costs, respectively. The table also provides value comparisons between the parcel UAV (Apt-70) and the passenger UAV (eCRM-300) use cases, including different types of costs and the average expected travel distance required to accomplish missions.

We observe that, for small parcel delivery UAVs, it is not sufficient to optimize the path only based on the economic cost, as doing so would result in much higher social and total costs. As shown in Table 5, when the decision maker only focuses on the economic cost with a weight combination of (1,0,0), the economic cost would decrease by around \$0.02 compared to the case under the total cost optimization with a weight combination of $(\frac{1}{3}, \frac{1}{3}, \frac{1}{3})$. However, such a negligible decrease in the economic cost would result in a \$0.18 increase in the social cost and a \$0.16 increase in the total cost. The above observation implies that identifying the optimal path solely based on economic cost minimization may not be the most effective strategy for parcel delivery missions. Such an objective is detrimental to both the social and economic considerations, as it cannot achieve a considerable decrease in the economic cost but significantly increases the non-economic cost. Hence, it is essential to plan paths for small parcel UAVs through total cost optimization. However, for the large passenger delivery UAVs, the conclusion is different based on the results. While path planning through total cost minimization is more cost-effective, it is sufficient to plan only through economic cost optimization. When decisions are made purely on economic cost minimization, the economic cost decreases by around \$0.15, while the total cost slightly increases by around \$0.17, only a 0.4% increase compared to the case under the total cost minimization. The environmental and social costs only increase by a small amount compared to the magnitude of the total cost incurred, around \$0.12 and \$0.19, respectively.

Studying the costs generated through the other two objectives, i.e., environmental and social objectives, we find that, for both small and large UAV delivery missions, the decision maker shall not plan UAV paths based on only environmental (weight combination of (0,1,0)) or social (weight combination of (0,0,1)) cost minimization as both are not economically sustainable. For example, for a passenger delivery mission, an optimization approach focused purely on minimizing environmental effects would reduce the environmental cost by \$32.3 while increasing other costs by about \$678.0. The above observation means that in an environmentally optimized framework, the decision maker is expected to incur a cost of \$21 for a \$1 decrease in environmental effects. Moreover, when the decision maker focuses on minimizing social impact, the social cost decreases by \$4.0, increasing other costs by \$644.9. In other words, in a social-optimized framework, the cost to reduce \$1 social cost is as high as \$163.3. Similarly, for small parcel delivery missions, a reduction of \$0.2 in environmental cost through environmental cost optimization would lead to an increase of \$8.3 dollar of the other costs, and a reduction of \$0.4 in social cost through social cost minimization would require an increase of \$4 in the other costs.

In summary, the decision maker should implement the total cost minimization approach for small UAVs such as Apt-70, as it balances economic, environmental, and social considerations by maintaining all the corresponding costs relatively low. On the other hand, for large UAVs similar to eCRM-003, while planning through total cost minimization is still the best choice, it is sufficient to optimize UAV paths through economic cost minimization. For both types of UAVs, the decision maker should not determine paths solely based on environmental or social objectives, as prioritizing such objectives would incur much higher other costs.

We further explore the impact of complex weightings or priorities assigned to the cost objectives, as illustrated in the last six rows of Table 5. Our findings indicate that, in general, assigning higher weights to the economic cost objective results in lower economic costs within the resulting cost distributions. For instance, when comparing the three weight combinations $(\frac{2}{4}, \frac{1}{4}, \frac{1}{4})$, $(\frac{1}{4}, \frac{2}{4}, \frac{1}{4})$, and $(\frac{1}{4}, \frac{1}{4}, \frac{1}{4})$ for both parcel and passenger delivery missions, we observe that the weight combination $(\frac{2}{4}, \frac{1}{4}, \frac{1}{4})$ yields the lowest economic costs. Similar observations can be made for other cost objectives. However, it is important to note that this relationship does not always hold. For instance, when comparing the weight combinations $(\frac{2}{4}, \frac{1}{4}, \frac{1}{4})$ and $(\frac{1}{3}, \frac{1}{3}, \frac{1}{3})$, it may seem that a higher weight is assigned to the economic objective in $(\frac{2}{4}, \frac{1}{4}, \frac{1}{4})$. However, we observe a lower resulting economic cost under the weight combination $(\frac{1}{3}, \frac{1}{3}, \frac{1}{3})$. These findings suggest that a monotonic relationship does not always exist between the weight assigned to a specific type of cost objective and the resulting cost in that category. This highlights the complex nature of the relationships between different costs, and emphasizes the need for an advanced decision support tool like the one proposed in this paper to better assist the decision-making process.

We also examine the influence of various cost weightings on the resultant paths, with a specific focus on the average expected travel distance required to accomplish missions. Our findings suggest that including economic costs in path establishment can decrease the anticipated travel distance. This observation applies to both types of use cases. For example, paths established solely on economic considerations tend to have the shortest average travel distances, which are 37.85 and 37.67 miles for parcel and passenger delivery, respectively. Conversely, when economic factors are disregarded in the path establishment process, it results in a longer average travel distance.

7. Conclusion

In this study, we develop a decision support system for UAV path planning under the consideration of stochastic weather evolution. More specifically, our proposed decision support system consists of a weather scenario generation algorithm that maps available ensemble-based weather forecast information to airspace blockage maps and a two-stage stochastic programming model that identifies safe and effective paths for UAV missions under weather uncertainty. Note that the proposed stochastic programming model involves an effective and accurate approach to a nonlinear problem, which can be tightly approximated and solved through discretization and linearization procedures. We then apply our method in two distinct use cases to obtain numerical insights on path planning decisions for both parcel and passenger UAV delivery services. We also explore the impact of weather uncertainty on path planning determinations and the total expected costs of given delivery missions. Moreover, we identify structural characteristics of how changes in various model parameters affect the total expected costs.

Compared to the deterministic path planning method, the average savings due to total expected cost reduction is around 6% when implementing the stochastic approach. In addition, such savings increase as weather conditions become more severe and complex. However, it is important to note that the stochastic method may not always be the optimal choice for operators. Making informed decisions requires careful consideration of trade-offs. Our proposed stochastic approach provides flexibility, risk mitigation, and optimal resource allocation; however, it also entails increased computational complexity and operator workload. On the other hand, deterministic path planning offers easy-to-implement and repeatable paths and requires lower computational efforts; however, it lacks adaptability to unexpected changes and may overlook the benefits of considering uncertainties. Furthermore, deterministic path planning can serve as a long-term decision tool by utilizing aggregated historical information, whereas stochastic path planning can be employed for short-term operational decisions. Operators should carefully assess their specific needs and operational requirements to determine the path-planning strategy that best aligns with their objectives.

Our numerical analysis also shows that establishing paths only based on economic cost minimization is not ideal for parcel delivery missions fulfilled by small UAVs, but is sufficient for passenger delivery missions done by large UAVs. As non-economic costs are nontrivial in missions delivered by small UAVs, decisions based on total cost minimization would be a better option with relatively low environmental and social cost levels. UAV paths shall not be determined solely through environmental or social objectives, as prioritizing these objectives would lead to much higher other costs. Furthermore, to reduce costs, decision makers should decrease the effective unit energy usage cost, unit cost of CO₂ emissions, unit cost of mission delay, unit noise cost, and/or increase the effective planned completion time. Moreover, operators should be careful about canceling missions. To avoid high cancellation costs, operators should either focus on offering delivery services within appropriate distances or shut down delivery services in regions facing severe weather conditions.

While our method effectively handles stochastic weather conditions, there is still a chance of encountering unforeseen weather events or sudden changes. Our current method incorporates the ability to cancel missions, including both in-advance and en-route cancellations, when weather conditions become severe and pose a risk to UAV operations. Additionally, to mitigate these risks, we can also offer UAV operators the flexibility to re-run our proposed method, allowing them to identify an alternative feasible path in response to unforeseen or sudden changes. Another viable approach is to enhance the frequency of re-routing, enabling more frequent updates to the path and reducing the likelihood of sudden changes.

Given the increasing application of UAVs in supply chain and transportation operations, the need for a safe and effective path planning supporting system is essential. Our proposed method can serve as a basis for future research in the area and help improve

efficiency and reduce costs of UAV operations for firms offering UAV-based parcel or passenger delivery services. For some potential extensions, it could be desirable to consider a 3D environment, and enable vertical path adjustments when more detailed weather information is available. Another interesting area for future research involves scaling up our methodology to accommodate a greater number of UAVs or more intricate mission scenarios. For instance, we only consider one destination for each mission in our current setting, i.e., a UAV delivers one package with a known destination each time. Therefore, we can expand our scope to encompass path planning for missions involving multiple packages/passengers and multiple destinations, as discussed in Chen et al. (2021). Related to this, we provide a detailed description of a potential scale-up of our methodology in Appendix S4.1.

Furthermore, en-route missions may be cancelled due to weather conditions, resulting in delivery failures and penalties such as mission cancellation costs. A relevant research question could be how to coordinate UAVs with existing public transportation systems (e.g., bus and truck) to tackle potential cancellations and deliver parcels/passengers to blocked areas to improve efficiency and reduce costs for the entire transportation system. A detailed discussion about the integration strategies for UAV services in existing transportation systems is provided in Appendix S4.2. Moreover, it is essential to conduct real tests to validate our findings and analysis, which currently can only be undertaken with FAA and NASA approval under actual weather conditions. To this end, we recommend performing UAV energy profiling experiments to test UAVs under various movement modes and calibrate UAV parameters for accurate calculations, In Appendix S4.4, we provide more information about obtaining FAA and NASA approval for field tests and the guidelines for conducting energy profiling experiments. Additionally, we suggest implementing both deterministic and our proposed stochastic path planning methods in real tests under varying natural weather conditions, followed by detailed energy and cost comparisons based on the collected data. Such experiments will provide valuable insights into the practical application of UAVs and help to refine our analysis further. To this end, the potential of incorporating our approach into the existing operating platforms utilized by FAA or NASA can also be considered. In Appendix S4.3, we identify and address the challenges associated with practical implementations of our approach. Successful incorporation necessitates interdisciplinary research and collaborations involving researchers, practitioners, and policymakers, which play a crucial role in bridging the gap between academia and industry. For example, the collaboration of academic researchers specializing in method development, industry practitioners with practical knowledge of UAV operations, and policymakers well-versed in regulatory frameworks can facilitate the development of comprehensive solutions. Through these collaborations, there is an exchange of expertise, insights, and best practices, which fosters the development of innovative path planning approaches that effectively tackle real-world challenges including dynamic obstacles, environmental constraints, and efficient resource utilization. By fostering such collaborations, academia and industry can collaboratively promote the adoption and implementation of UAV path planning solutions, revolutionizing various industries, including logistics, transportation, agriculture, and disaster management.

Declaration of competing interest

The authors declare that they have no known competing financial interests or personal relationships that could have appeared to influence the work reported in this paper.

Acknowledgment

The work presented in this article was in part supported by NSF award #2018074, a University of Massachusetts Interdisciplinary Research Award, and by Jerome M. and Linda L. Paros whose generosity established the Paros Center for Atmospheric Research. The authors are also thankful to Apoorva Bajaj for his contributions during the early stages of this project.

Appendix A. Supplementary data

Supplementary material related to this article can be found online at https://doi.org/10.1016/j.tre.2023.103314. Supporting information includes:

Appendix S1. Summary of Notations Used

Appendix S2. Practicality and Necessity of Our Stochastic Approach

Appendix S3. Validation for the Weather Scenario Generation Algorithm

Appendix S4. Potential Extensions and Practical Implementations

References

Aggarwal, S., Kumar, N., 2020. Path planning techniques for unmanned aerial vehicles: A review, solutions, and challenges. Comput. Commun. 149, 270–299. Ahmed, S., Mohamed, A., Harras, K., Kholief, M., Mesbah, S., 2016. Energy efficient path planning techniques for UAV-based systems with space discretization. In: 2016 IEEE Wireless Communications and Networking Conference. IEEE, pp. 1–6.

Aiello, G., Inguanta, R., D'Angelo, G., Venticinque, M., 2021. Energy consumption model of aerial urban logistic infrastructures. Energies 14 (18), 5998.

Allon, G., Federgruen, A., Pierson, M., 2011. How much is a reduction of your customers' wait worth? An empirical study of the fast-food drive-thru industry

based on Structural estimation methods. Manuf. Serv. Oper. Manag. 13 (4), 489–507.

Arribas, A., Robertson, K., Mylne, K., 2005. Test of a poor man's ensemble prediction system for short-range probability forecasting. Mon. Weather Rev. 133 (7), 1825–1839.

Battan, L.J., 1953. Duration of convective radar cloud units. Bull. Am. Meteorol. Soc. 34, 227-228.

Bell, 2021a. Bell APT. URL https://www.bellflight.com/products/bell-apt. Retrieved July 16, 2021.

Bell, 2021b. Bell's Autonomous Pod Transport demonstrates game changing aerial resupply feature. URL https://rb.gy/4c1k. Retrieved March 12, 2023.

Blasi, L., D'Amato, E., Mattei, M., Notaro, I., 2020. Path planning and real-time collision avoidance based on the essential visibility graph. Appl. Sci. 10 (16),

Campbell, J.F., Sweeney, D., Zhang, J., 2017a. Strategic Design for Delivery with Trucks and Drones. Supply Chain Analytics Report SCMA (04 2017).

CASA, 2020. DFW urban test bed. URL https://shorturl.at/avAVY. Retrieved Sep 22, 2023.

CASA, 2022. CASA UAV path planning. URL https://emmy9.casa.umass.edu/casauam/stochastic.html. Retrieved Sep 26, 2023.

Chang, Y.-H., Solak, S., Clarke, J.-P.B., Johnson, E.L., 2016. Models for single-sector stochastic air traffic flow management under reduced airspace capacity. J. Oper. Res. Soc. 67 (1), 54–67.

Charlton, A., 2020. Will flying taxis become a reality? 10 companies (still) preparing for takeoff. URL https://www.gearbrain.com/10-flying-car-companies-2587872239.html. Retrieved March 18, 2021.

Chen, H., Hu, Z., Solak, S., 2021. Improved delivery policies for future drone-based delivery systems. European J. Oper. Res. 294 (3), 1181-1201.

Chen, T., Zhang, G., Hu, X., Xiao, J., 2018. Unmanned aerial vehicle route planning method based on a star algorithm. In: 2018 13th IEEE Conference on Industrial Electronics and Applications (ICIEA). IEEE, pp. 1510–1514.

Christian, A.W., Cabell, R., 2017. Initial investigation into the psychoacoustic properties of small unmanned aerial system noise. In: 23rd AIAA/CEAS Aeroacoustics Conference. p. 4051.

Chung, S.H., Sal, B., Lee, J., 2020. Optimization for drone and drone-truck combined operations: A review of the state of the art and future directions. Comput. Oper. Res. 123, 105004.

Citroni, R., Di Paolo, F., Livreri, P., 2019. A novel energy harvester for powering small UAVs: Performance analysis, model validation and flight results. Sensors 19 (8), 1771.

Clarke, J.-P.B., Solak, S., Ren, L., Vela, A.E., 2013. Determining stochastic airspace capacity for air traffic flow management. Transp. Sci. 47 (4), 542-559.

D'Amato, E., Mattei, M., Notaro, I., 2019. Bi-level flight path planning of UAV formations with collision avoidance. J. Intell. Robot. Syst. 93 (1-2), 193-211.

D'Andrea, R., 2014. Guest editorial can drones deliver? IEEE Trans. Autom. Sci. Eng. 11 (3), 647-648.

Darbari, V., Gupta, S., Verma, O.P., 2017. Dynamic motion planning for aerial surveillance on a fixed-wing UAV. In: 2017 International Conference on Unmanned Aircraft Systems (ICUAS). IEEE, pp. 488–497.

De Waen, J., Dinh, H.T., Torres, M.H.C., Holvoet, T., 2017. Scalable multirotor UAV trajectory planning using mixed integer linear programming. In: 2017 European Conference on Mobile Robots (ECMR). IEEE, pp. 1–6.

DJI, 2023. DJI SPEC. URL https://www.dji.com/mini-3-pro/specs. Retrieved March 23, 2023.

Du, W., Guo, T., Chen, J., Li, B., Zhu, G., Cao, X., 2021. Cooperative pursuit of unauthorized UAVs in urban airspace via Multi-agent reinforcement learning. Transp. Res. C 128, 103122.

EASA, 2019. European Aviation Environmental Report 2019. Tech. rep., European Environment Agency, European Union Aviation Safety Agency, Eurocontrol. Electric Choice, 2021. Instantly see the electric rates and plans available to your home or business. URL https://www.electricchoice.com/electricity-prices-by-state/. Retrieved July 16, 2021.

EPA, 2021a. Emissions & generation resource integrated database (eGRID). URL https://www.epa.gov/egrid. Retrieved July 16, 2021.

EPA, 2021b. Greenhouse gas equivalencies calculator - revision history. URL https://www.epa.gov/energy/greenhouse-gas-equivalencies-calculator-revision-history. Retrieved July 16, 2021.

Eurocontrol, 2020. Eurocontrol Standard Inputs for Economic Analyses. Tech. rep., European Organisation for the Safety of Air Navigation.

EVTOL, 2021. Bell autonomous pod transport. URL https://evtol.news/bellapt/. Retrieved July 16, 2021.

FAA, 2020. Small unmanned aircraft systems (UAS) regulations (Part 107). URL https://www.faa.gov/news/fact_sheets/news_story.cfm?newsId=22615. Retrieved July 16, 2021.

FAA, 2020. UAM concept of operations (ConOps) version 1.0 with both internal and external stakeholders. URL https://nari.arc.nasa.gov/sites/default/files/attachments/UAM_ConOps_v1.0.pdf. Retrieved March 10, 2021.

FAA, 2021. Operations over people general overview. URL https://www.faa.gov/uas/commercial_operators/operations_over_people/. Retrieved May 10, 2021.

FAA, 2023. Recreational flyers & community-based organizations. URL https://www.faa.gov/uas/recreational_flyers. Retrieved March 23, 2023.

Ferguson, J., Kara, A.Q., Hoffman, K., Sherry, L., 2013. Estimating domestic US airline cost of delay based on European model. Transp. Res. C 33, 311–323. Foote, G.B., Mohr, C.G., 1979. Results of a randomized hail suppression experiment in Northeast Colorado. Part VI: Post hoc stratification by storm intensity and type. J. Appl. Meteorol. Climatol. 18 (12), 1589–1600.

Franco, A., Rivas, D., Valenzuela, A., 2018. Optimal aircraft path planning in a structured airspace using ensemble weather forecasts. Sesar Innov. Days 2018, 1-7

Gagliardi, P., Teti, L., Licitra, G., 2018. A statistical evaluation on flight operational characteristics affecting aircraft noise during take-off. Appl. Acoust. 134, 8–15

Gao, M., Hugenholtz, C.H., Fox, T.A., Kucharczyk, M., Barchyn, T.E., Nesbit, P.R., 2021. Weather constraints on global drone flyability. Sci. Rep. 11 (1), 1–13. Goodchild, A., Toy, J., 2018. Delivery by drone: An evaluation of unmanned aerial vehicle technology in reducing CO2 emissions in the delivery service industry. Transp. Res. D 61, 58–67.

Guerriero, F., Surace, R., Loscri, V., Natalizio, E., 2014. A multi-objective approach for unmanned aerial vehicle routing problem with soft time windows constraints. Appl. Math. Model. 38 (3), 839–852.

Hassanalian, M., Abdelkefi, A., 2017. Classifications, applications, and design challenges of drones: A review. Prog. Aerosp. Sci. 91, 99-131.

He, L., Aouf, N., Song, B., 2021. Explainable Deep Reinforcement Learning for UAV autonomous path planning. Aerosp. Sci. Technol. 118, 107052.

He, X., He, F., Li, L., Zhang, L., Xiao, G., 2022. A route network planning method for urban air delivery. Transp. Res. E 166, 102872.

Holden, J., Goel, N., 2016. Fast-forwarding to a future of on-demand urban air transportation. URL https://evtol.news/_media/PDFs/UberElevateWhitePaperOct2016.pdf. Retrieved July 16, 2021.

Industrial Distribution, 2016. DHL successfully tests delivery helicopter drone in Bavarian Alps. URL https://rb.gy/cykcke. Retrieved March 23, 2023.

Jiang, X., Zhou, Q., Ye, Y., 2017. Method of task assignment for UAV based on particle swarm optimization in logistics. In: Proceedings of the 2017 International Conference on Intelligent Systems, Metaheuristics & Swarm Intelligence. pp. 113–117.

Karaman, S., Inalhan, G., 2008. Large-scale task/target assignment for UAV fleets using a distributed branch and price optimization scheme. IFAC Proc. Vol. 41 (2), 13310–13317.

Kirschstein, T., 2020. Comparison of energy demands of drone-based and ground-based parcel delivery services. Transp. Res. D 78, 102209.

Leutbecher, M., Palmer, T.N., 2008. Ensemble forecasting. J. Comput. Phys. 227 (7), 3515–3539.

Levinson, D., Kanafani, A., Gillen, D., 1999. Air, high-speed rail, or highway: A cost comparison in the California corridor. Transp. Q. 53, 123-131.

Li, S., Zhang, H., Li, Z., Liu, H., 2021. An air route network planning model of logistics UAV terminal distribution in urban low altitude airspace. Sustainability 13 (23), 13079.

Liu, H., Li, X., Fan, M., Wu, G., Pedrycz, W., Nagaratnam Suganthan, P., 2022. An autonomous path planning method for unmanned aerial vehicle based on a tangent intersection and target guidance strategy. IEEE Trans. Intell. Transp. Syst. 23 (4), 3061–3073.

Lu, C., Yuan, H., Schwartz, B.E., Benjamin, S.G., 2007. Short-range numerical weather prediction using time-lagged ensembles. Weather Forecast. 22 (3), 580–595.

Luna, M.A., Ale Isaac, M.S., Ragab, A.R., Campoy, P., Flores Peña, P., Molina, M., 2022. Fast multi-UAV path planning for optimal area coverage in aerial sensing applications. Sensors 22 (6), 2297.

Luo, Y., Yu, Y., Jin, Z., Li, Y., Ding, Z., Zhou, Y., Liu, Y., 2020. Privacy-aware UAV flights through self-configuring motion planning. In: 2020 IEEE International Conference on Robotics and Automation (ICRA). IEEE, pp. 1169–1175.

Mag, V., 2020. Bell's APT 70 multicopter completes first BVLOS flight. URL https://verticalmag.com/news/bells-apt-70-multicopter-completes-first-bvlos-flight/.

Retrieved March 12, 2023.

Maibach, M., Schreyer, C., Sutter, D., Van Essen, H., Boon, B., Smokers, R., Schroten, A., Doll, C., Pawlowska, B., Bak, M., 2008. Handbook on Estimation of External Costs in the Transport Sector, Vol. 336. CE Delft.

Maple, C., 2003. Geometric design and space planning using the marching squares and marching cube algorithms. In: Proceedings 2003 International Conference on Geometric Modeling and Graphics. pp. 90–95.

McGuire, M., Rys, M.J., Rys, A., et al., 2016. A Study of How Unmanned Aircraft Systems Can Support the Kansas Department of Transportation's Efforts to Improve Efficiency, Safety, and Cost Reduction. Tech. rep., Kansas. Dept. of Transportation.

Miao, Y., Zhong, L., Yin, Y., Zou, C., Luo, Z., 2017. Research on dynamic task allocation for multiple unmanned aerial vehicles. Trans. Inst. Meas. Control 39 (4), 466–474.

Mlot, S., 2022. Amazon begins testing drone deliveries in California, Texas. URL https://rb.gy/nykgfi. Retrieved March 23, 2023.

Moon, S., Oh, E., Shim, D.H., 2013. An integral framework of task assignment and path planning for multiple unmanned aerial vehicles in dynamic environments. J. Intell. Robot. Syst. 70 (1), 303–313.

NSSL, 2023. Severe weather 101. URL http://rb.gy/jlye. Retrieved March 23, 2023.

Otto, A., Agatz, N., Campbell, J., Golden, B., Pesch, E., 2018. Optimization approaches for civil applications of unmanned aerial vehicles (UAVs) or aerial drones: A survey. Networks 72 (4), 411–458.

Pasztor, A., Ferek, K., 2021. FAA approves first fully automated commercial drone flights. URL https://www.wsj.com/articles/faa-approves-first-fully-automated-commercial-drone-flights-11610749377. Retrieved May 6, 2021.

Pehlivanoglu, Y.V., 2012. A new vibrational genetic algorithm enhanced with a Voronoi diagram for path planning of autonomous UAV. Aerosp. Sci. Technol. 16 (1), 47–55.

Porsche Consulting, 2018. The future of vertical mobility. URL shorturl.at/sIQU0. Retrieved July 16, 2021.

Radhakrishnan, C., Chandrasekar, V., 2020. CASA prediction system over Dallas–Fort Worth urban network: Blending of nowcasting and high-resolution numerical weather prediction model. J. Atmos. Ocean. Technol. 37 (2), 211–228.

Rafanavicius, V., Cimmperman, P., Taluntis, V., Man, K.L., Volkvicius, G., Jurkynas, M., Bezaras, J., 2017. Efficient path planning methods for UAVs inspecting power lines. In: 2017 International Conference on Platform Technology and Service (PlatCon). IEEE, pp. 1–6.

Ranquist, E., Steiner, M., Argrow, B., 2017. Exploring the range of weather impacts on UAS operations. In: 18th Conference on Aviation, Range, and Aerospace Meteorology. pp. 1–11.

Ren, L., Chang, D., Solak, S., Clarke, J.-P.B., Barnes, E., Johnson, E., 2007. Simulating air traffic blockage due to convective weather conditions. In: 2007 Winter Simulation Conference. IEEE, pp. 1897–1904.

Rizzi, S.A., Huff, D.L., Boyd, D.D., Bent, P., Henderson, B.S., Pascioni, K.A., Sargent, D.C., Josephson, D.L., Marsan, M., He, H.B., et al., 2020. Urban Air Mobility Noise: Current Practice, Gaps, and Recommendations. Tech. rep., National Aeronautics and Space Administration, Langley Research Center.

Roseman, C.A., Argrow, B.M., 2020. Weather hazard risk quantification for sUAS safety risk management. J. Atmos. Ocean. Technol. 37 (7), 1251-1268.

Saha, S., Vasegaard, A.E., Nielsen, I., Hapka, A., Budzisz, H., 2021. UAVs path planning under a Bi-objective optimization framework for smart cities. Electronics 10 (10), 1193.

Salama, M.R., Srinivas, S., 2022. Collaborative truck multi-drone routing and scheduling problem: Package delivery with flexible launch and recovery sites. Transp. Res. E 164, 102788.

Samà, M., D'Ariano, A., D'Ariano, P., Pacciarelli, D., 2014. Comparing centralized and rolling horizon approaches for optimal aircraft traffic control in terminal areas. Transp. Res. Res. 2449 (1), 45–52.

Shen, L., Wang, Y., Liu, K., Yang, Z., Shi, X., Yang, X., Jing, K., 2020. Synergistic path planning of multi-UAVs for air pollution detection of ships in ports. Transp. Res. E 144, 102128.

Song, B.D., Kim, J., Morrison, J.R., 2016. Rolling horizon path planning of an autonomous system of UAVs for persistent cooperative service: MILP formulation and efficient heuristics. J. Intell. Robot. Syst. 84 (1–4), 241–258.

Steiner, M., Bateman, R., Benjamin, S., Brown, B., Carmichael, B., Davidson, G., Krozel, J., Mahoney, J., Mueller, C., Pinto, J., et al., 2008. Integration of probabilistic weather information with air traffic management decision support tools: A conceptual vision for the future. In: 13th Conference on Aviation, Range and Aerospace Meteorology. pp. 1–9.

Stolaroff, J.K., Samaras, C., O'Neill, E.R., Lubers, A., Mitchell, A.S., Ceperley, D., 2018. Energy use and life cycle greenhouse gas emissions of drones for commercial package delivery. Nature Commun. 9 (1), 1–13.

Thibbotuwawa, A., Bocewicz, G., Radzki, G., Nielsen, P., Banaszak, Z., 2020. UAV mission planning resistant to weather uncertainty. Sensors 20 (2), 515.

Thibbotuwawa, A., Nielsen, P., Zbigniew, B., Bocewicz, G., 2018. Energy consumption in unmanned aerial vehicles: A review of energy consumption models and their relation to the UAV routing. In: International Conference on Information Systems Architecture and Technology. Springer, pp. 173–184.

Tong, G., Jiang, N., Biyue, L., Xi, Z., Ya, W., Wenbo, D., 2021. UAV navigation in high dynamic environments: A deep reinforcement learning approach. Chin. J. Aeronaut. 34 (2), 479–489.

Torija, A.J., Li, Z., Self, R.H., 2020. Effects of a hovering unmanned aerial vehicle on urban soundscapes perception. Transp. Res. D 78, 102195.

Uber Elevate, 2021. Uber Elevate eCRM-003. URL https://evtol.news/uber-elevate-ecrm-003/. Retrieved July 16, 2021.

Uber Elevate, 2023. XPeng AeroHT Voyager X1. URL https://evtol.news/xpeng-aeroht-voyager-x1. Retrieved March 23, 2023.

Van Essen, H., van Wijngaarden, L., Schroten, A., Sutter, D., Bieler, C., Maffii, S., Brambilla, M., Fiorello, D., Fermi, F., Parolin, R., et al., 2019. Handbook on the External Costs of Transport. 18.4 K83. 131. European Commission.

Vera, S., Cobano, J.A., Heredia, G., Ollero, A., 2016. Collision avoidance for multiple UAVs using rolling-horizon policy. J. Intell. Robot. Syst. 84 (1), 387–396. Wang, Z., Sheu, J.-B., 2019. Vehicle routing problem with drones. Transp. Res. B 122, 350–364.

Welch, A., 2015. A Cost-Benefit Analysis of Amazon Prime Air. Tech. rep., University of Tennessee at Chattanooga.

Wing, 2023. Wing delivery is easy to use. URL https://wing.com/how-it-works/. Retrieved March 16, 2023.

World Bank, 2021. Carbon pricing dashboard. URL https://carbonpricingdashboard.worldbank.org/map_data. Retrieved July 16, 2021.

Yahoo Finance, 2021. Global commercial UAV market report 2021–2026. URL https://finance.yahoo.com/news/global-commercial-uav-market-report-144000158. html. Retrieved May 6, 2021.

Yan, C., Wang, C., Xiang, X., Low, K.H., Wang, X., Xu, X., Shen, L., 2023. Collision-avoiding flocking with multiple fixed-wing UAVs in obstacle-cluttered environments: A task-specific curriculum-based MADRL approach. IEEE Trans. Neural Netw. Learn. Syst..

Yang, L., Qi, J., Xiao, J., Yong, X., 2014. A literature review of UAV 3D path planning. In: Proceeding of the 11th World Congress on Intelligent Control and Automation. IEEE, pp. 2376–2381.

Yao, J., You, F., 2020. Simulation-based optimization framework for economic operations of autonomous electric taxicab considering battery aging. Appl. Energy 279, 115721.

Yin, C., Xiao, Z., Cao, X., Xi, X., Yang, P., Wu, D., 2017. Offline and online search: UAV multiobjective path planning under dynamic urban environment. IEEE Internet Things J. 5 (2), 546–558.

- Yu, X., Chen, W.-N., Gu, T., Yuan, H., Zhang, H., Zhang, J., 2018. ACO-A*: Ant colony optimization plus A* for 3-D traveling in environments with dense obstacles. IEEE Trans. Evol. Comput. 23 (4), 617–631.
- Yu, H., Meier, K., Argyle, M., Beard, R.W., 2014. Cooperative path planning for target tracking in urban environments using unmanned air and ground vehicles. IEEE/ASME Trans. Mechatronics 20 (2), 541–552.
- Zhai, W., Han, B., Li, D., Duan, J., Cheng, C., 2021. A low-altitude public air route network for UAV management constructed by global subdivision grids. PLoS One 16 (4), e0249680.
- Zhan, X., Szeto, W., Chen, X.M., 2022. A simulation-optimization framework for a dynamic electric ride-hailing sharing problem with a novel charging strategy. Transp. Res. E 159, 102615.
- Zohar, S., 2018. The True Cost of Declined Orders. Riskified Blog, (June 17).